STRUCTURAL AND MAGNETIC PROPERTIES OF Si(100)/Ta/Co MULTILAYERS FOR SPINTRONICS APPLICATIONS

A Thesis Submitted to
the Graduate School of Engineering and Sciences of
İzmir Institute of Technology
in Partial Fulfillment of the Requirements for the Degree of

MASTER OF SCIENCE

in Physics

by
Kadir VAHAPLAR

July 2007
İZMİR

We approve the thesis of **Kadir VAHAPLAR**

Date of Signature

..... **13 July 2007**
Assist. Prof. Dr. Süleyman TARI
Supervisor
Department of Physics
İzmir Institute of Technology

..... **13 July 2007**
Assoc. Prof. Dr. Metin TANOĞLU
Department of Mechanical Engineering
İzmir Institute of Technology

..... **13 July 2007**
Assoc. Prof. Dr. Salih OKUR
Department of Physics
İzmir Institute of Technology

..... **13 July 2007**
Assist. Prof. Dr. Yusuf SELAMET
Head of the Department
İzmir Institute of Technology

.....
Prof. Dr. M. Barış ÖZERDEM
Head of the Graduate School

ACKNOWLEDGEMENTS

First of all, I am grateful to my supervisor Assist. Prof. Dr. Süleyman TARI for his positive attitude and inspiration at all stages of my thesis. I sincerely thank him for his patience and motivating me throughout this study. I also thank Assoc. Prof. Dr. Lütfi ÖZYÜZER for his valuable suggestions during my research work.

My thanks also go to the staff of the Center for Material Research of İzmir Insitute of Technology for helping me in performing the analysis of my experiments. Additionally, I would like to thank Assoc. Prof. Dr. Salih OKUR for the AFM measurements. I also thankfully acknowledge İzmir Institute of Technology for providing me a research assistantship and TUBITAK for funding the project "TBAG-105T109" during my thesis.

I express my sincere gratitude to my family for their continuous support in all aspects. I would like to have the same kind of motivation and support from them forever. My special thanks go to my girlfriend, Layka. She introduced an abundance of love and enjoyment into my life and has always been there for me.

Lastly, I am very thankful to my lab mates and friends at IYTE, especially Kaan Oğuz, Savaş Ulucan, Yılmaz Şimşek and Hüseyin Tokuç, who made my stay memorable and enjoyable.

ABSTRACT

STRUCTURAL AND MAGNETIC PROPERTIES OF Si(100)/Ta/Co MULTILAYERS FOR SPINTRONICS APPLICATIONS

This thesis is concerned with the structural and magnetic properties of Si(100)/Ta/Co single and multilayer thin films grown by DC magnetron sputtering technique. The structural properties of the films have been studied by X-Ray Diffractometer (XRD), Atomic Force Microscopy (AFM) and Scanning Electron Microscopy (SEM). This study revealed that a single Co film grows amorphous on silicon substrate up to 50 nm at room temperature. After this thickness, Co starts crystallizing in hexagonal (002) plane. The same crystallinity was also observed for 25 nm amorphous Co which was annealed at 450^0C at high vacuum for 30 minutes. The presence of a single crystalline tetragonal Ta phase (β-Ta) with the orientation along (002) has been observed for 40 nm Ta growth on silicon substrate. The Si(100)/Ta/Co bilayers and multilayers show good crystallinity for both Ta and Co films. SEM and AFM results show that all the single and multilayers grew uniform, continuous and with very low surface roughness.

The magnetic properties of the films were investigated using Vibrating Sample Magnetometer (VSM), by measuring hysteresis loops. The effects of the thickness and growth pressure on the magnetic properties of Co films were studied. The easy magnetization axis of the samples is found to be parallel to the Co film plane. As the Co film thickness increased from 4 nm to 15 nm, the coercivity (H_c) decreased from 72 G to 20 G and after a threshold thickness it increased almost linearly up to 180 G for 100 nm film while the magnetization decreased. Moreover, it has been observed that as the Co growth pressure increases, the H_c value of Co films increases. Finally, we obtained two different H_c values for our MTJ sandwich with the structure of Si(100)/Ta/Co/TaO_x/Co/Ta.

ÖZET

SPİNTRONİK UYGULAMALARI İÇİN Si(100)/Ta/Co ÇOKLU KATMANLARIN YAPISAL VE MANYETİK ÖZELLİKLERİ

Bu tez, DC mıknatıssal sıçratma tekniği kullanılarak üretilen Si(100)/Ta/Co tek ve çoklu katman ince filimlerin yapısal ve manyetik özellikleriyle ilgilidir. Filimlerin yapısal özellikleri XRD, AFM ve SEM kullanılarak incelenmiştir. Bu çalışmadan, oda sıcaklığında silikon alttaş üserine büyütülen Co filimin 50 nm'ye kadar amorf bir yapıya sahip olduğu anlaşılmıştır. Bu kalınlıktan sonra hegzagonal (002) düzlemi doğrultusunda kristallenmeye başlamıştır. Kristallenme, 25 nm'lik amorf filim 450-^{0}C'de yüksek vakum ortamında 30 dakika tavlandıktan sonra da görülmüştür. 40 nm kalınlığındaki Ta filimin silikon alttaş üzerine (002) düzlemi doğrultusunda tek kristal ve tetragonal Ta fazda (β-Ta) büyüdüğü görülmüştür. Si(100)/Ta/Co çift katmanlı ve çoklu katmanlı yapılar, Ta ve Co için iyi kristallenme göstermiştir. SEM ve AFM sonuçlarıyla, bütün tek ve çoklu katmanların düzenli, sürekli ve çok az pürüzlülükle büyüdükleri görülmüştür.

VSM ile histeresis döngüleri ölçülerek filimlerin manyetik özellikleri incelenmiştir. Filim kalınlığının ve büyüme basıncının Co filimin manyetik özelliklerine etkileri çalışılmıştır. Örneklerin kolay manyetizasyon eksenlerinin Co film yüzeyine paralel olduğu görülmüştür. Co filim kalınlığı 4 nm'den 15 nm'ye arttırıldığında artık mıknatıslanım değeri (H_c) 72 G'dan 20 G'a düşmüştür ve eşik kalınlık değerinden sonra 100 nm'ye (180 G) kadar neredeyse lineer olarak artarken manyetizasyon değerinin de düştüğü görülmüştür. Buna ek olarak, Co filimin büyütme basıncı arttırıldığında, H_c değerinin arttığı gözlenmiştir. Son olarak, Si(100)/Ta/Co/TaO_x/ Co/Ta manyetik tünel eklemi yapısında iki farkli H_c değeri elde edilmiştir.

TABLE OF CONTENTS

LIST OF FIGURES

LIST OF TABLES

CHAPTER 1

INTRODUCTION

Spintronics, or spin electronics, is an attractive field of basic and applied research in physics and engineering that aims to use the role played by electron spin in solid state materials (Wu et al. 2003). Spintronic devices make use of spin properties instead of, or in addition to electron charge to carry information. Use of electron spin to store, transport and manipulate information would have many specified advantages. These include greater data processing speed, low power consumption and non-volatility. "Non-volatility" means that the data are still encoded when the power is switched off (Barthélémy et al. 2002).

The name of spintronics is nowadays used to describe the field of research on electronic devices in which the electron spin plays the role of the active element (Prinz 1998). The first observation showing that the spin can affect electron transport was in 1857 when the anisotropic magnetoresistance (AMR) effect was reported (Thomson 1856). AMR shows that the resistance of a metallic ferromagnet depends on the angle between the magnetization and current direction (Rijks et al. 1995). This relative resistance change is called magnetoresistance (MR) ratio, and the maximum value observed at room temperature is ~5%.

More than 100 years later, in 1988, Baibich and coworkers (Baibich et al. 1988) and Binasch and coworkers (Binasch et al. 1989), discovered a larger resistance change upon applying a magnetic field in multilayers of magnetic layers separated by nonmagnetic metal layers and called it giant magnetoresistance (GMR) effect. The origin of this effect is due to spin dependent electron scattering. The total current is the result of two parallel currents, one due to spin up and one due to spin down electrons. The resistances experienced by these two currents are generally different and depend on the alignment of the magnetization direction of the ferromagnetic (FM) layers. The direction of the magnetization of one layer is pinned in one direction and the other, the free layer, is free to rotate in the direction of the external magnetic field. This simple three layer structure is called *spin valve*. By applying an external magnetic field, the orientation of the magnetization of the FM layers can be changed from parallel to

antiparallel. A low resistance is obtained if the magnetizations of the two layers are parallel and a high resistance if they are anti-parallel, as is indicated in Figure 1.1.

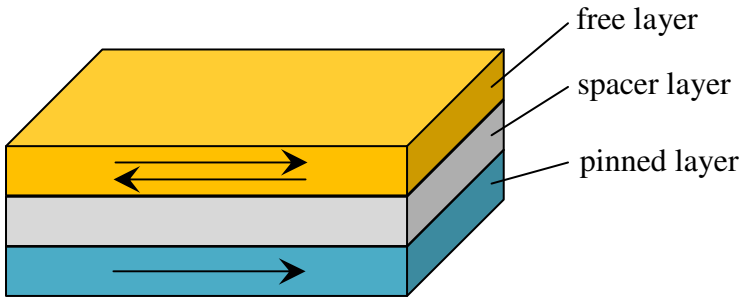

Figure 1.1. Simple spin valve structure.

Spin-valves reached market in 1998 when they were introduced for the first time in disk drives by IBM. Since then, this technology became the standard for read heads. Spin-valves can be viewed as sensitive magnetic field sensors. They may also be used in other applications: measurement of electrical current, position or rotation encoders, magnetoresistive compass, and magnetoresistive heads for video-tapes or other storage media.

The next generation of spintronic devices and the main topic of this thesis are *magnetic tunnel junctions* (MTJs). A magnetic tunnel junction consists of two magnetic layers separated by an insulator. The insulator is so thin, that electrons have a small probability to go from one electrode to the other through the barrier. This quantum mechanical process is called *tunneling* and is due to the wave character of the electron. For a magnetic tunnel junction, the conductivity is found to depend on the relative orientation of the magnetizations. The origin of this effect is that the tunnel probability of an electron to tunnel through the barrier depends on the wave length or the energy of the electron. In ferromagnetic materials the energy of spin-up and spin-down electrons are different and this lead to a spin dependent tunnel probability. By reversing the magnetization the energy of spin-up and spin-down electrons in the reversed layer are interchanged, as is shown schematically in Figure 1.2(b). This leads to a resistance difference, which is called *tunneling magnetoresistance* (TMR), between parallel and antiparallel magnetized layers.

TMR ratio is calculated by the formula;

$$TMR \equiv \left(\frac{R_{ap} - R_p}{R_p} \right) \times 100$$

In this expression, R_{ap} and R_p represent the anti-parallel alignment resistance and parallel alignment resistance values of the multilayer, respectively.

Although this effect was already found in 1975 (Julliere 1975), only since 1995 a reproducible fabrication process was developed (Moodera et al. 1995). TMR ratio was achieved up to 500% at room temperature for CoFeB/MgO/CoFeB structure (Lee et al. 2007). The variation of the resistance of these devices is the same with spin valve device as shown in Figure 1.1.

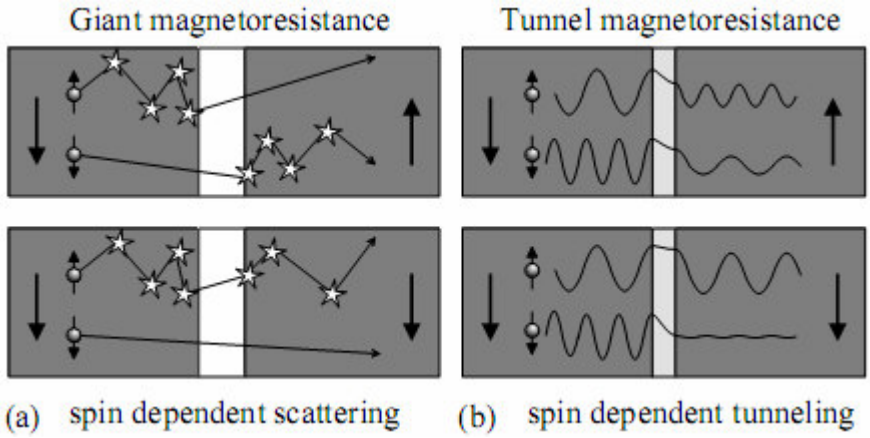

Figure 1.2. Principles of transport of electrons through a GMR device (a) and tunnel junction (b). The magnetization directions of magnetic materials are indicated by an arrow (Smits 2001).

Most magnetoresistive devices depend on thin-film technology for their creation. Since the electronic properties of the films may depend strongly on the physical structure, it is very important to be able to determine and analyze the exact structural properties of the films. Also, by varying the structure of the materials and studying the changes in device behavior, the detailed physics behind the behavior may be studied.

In a magnetic tunnel junction, a bottom electrode, including the exchange bias layer, is grown on a substrate. Then the barrier layer is grown, followed by the top

electrode. A capping layer can also be deposited on the top electrode in order to prevent oxidation. The insulating layer, which is most often Al_2O_3 (Moodera 1995, Mitsuzuka 1999, Wang 2004), can be created by naturally oxidizing the metal layer or direct deposition of Al_2O_3, for instance by reactive sputtering.

In order to have high TMR values, the barrier must be homogeneous, pinholes free and have low impurities. Layers must be smooth because some roughness can cause in homogeneous currents through the layers that can lead to local heating and creating shorts. Roughness of the barrier can also cause a magnetic coupling between the two electrodes, which results in the situation that the layers do not switch independently and antiparallel state cannot be achieved anymore (Knechten 2004).

In this study, we first grew Ta film as a buffer layer on silicon substrate because the buffer layer can improve the flatness of the multilayer, and a greater degree of smoothness can be obtained (Ma and Wong 2002). It is also used as bottom contact layer for magnetoresistance measurements. Co films were grown on Si and Ta with different thicknesses and pressures to investigate structural and magnetic properties of grown layers. Finally, as a first attempt towards growing MTJ structures, Si/Ta/Co/TaO_x/Co/Ta was grown and magnetic properties were studied.

CHAPTER 2

THIN FILM DEPOSITION

The process of sputter deposition for the production of thin films in various applications has increased widely in popularity. This is because of its ease of operation, accurate control of the growth rate, excellent film adhesion and a high degree of reproducibility of the deposited films.

All layers were deposited by magnetron sputtering technique. Therefore, a short overview of sputtering process will be given. Then, the magnetism of thin films as well as the dependence of magnetic behavior on structural properties will be discussed. An overview of material properties is also presented briefly.

2.1. Sputtering Process

Among the numerous techniques available today for depositing thin films, sputter deposition is one of the most capable techniques to prepare thin films almost any material. Some of the advantages of sputtering are: high uniformity of deposited films, good adhesion to the substrate, better reproducibility of films and simplicity of film thickness control.

This method consists of the bombardment of the target material by fast moving, heavy, inert gas ions (usually Ar^+ ions) from a plasma. The bombarding ions cause atoms to be ejected from the target material by momentum transfer between the colliding ions and the target atoms. The basic schematic for a DC sputtering system is schematically shown in Fig. 2.1, where some processes are shown to occur when the ions collide with the target material. In magnetron sputtering process permanent magnets are placed under the target to create a magnetic field close to the surface of the target. Secondary electrons, which are trapped by this magnetic field, join the plasma and cause the continuous ionization of the gas in order to increase ions needed for sputtering. They also release their energy in the form of heat on the substrate. The mobility of the incident atoms arriving at the substrate depends on the sputtering parameters (power, pressure), the temperature of the substrate, the distance between the target and the substrate, and the surface of the substrate itself.

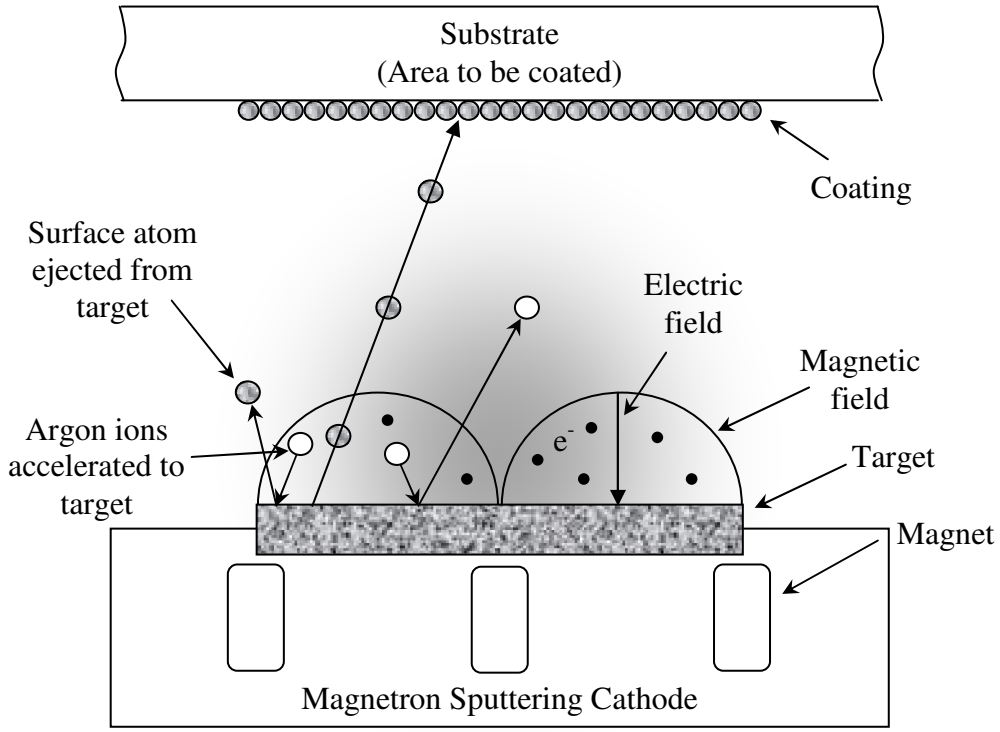

Figure 2.1. Schematic explaining the sputtering process.

The magnetic and structural properties of thin films are strongly dependent upon the deposition process and the growth parameters. Careful control of the sputtering parameters is essential to prevent the films suffering from residual stresses and columnar growth which can affect both the magnetic and structural properties.

The kinetics of the sputtering process and the mobility of the sputtered atoms at the surface of the substrate determine the final structural and magnetic properties of the thin films. Some factors which influence these processes are explained briefly below:

Pressure: The pressure of the sputtering gas not only provides the inert gas ions needed for the sputtering process of the target, but also acts as a moderator for the ejected atoms from the target. At low pressures, the sputtered atoms have much higher energies than the plasma gas between the target and substrate. The sputtered atoms in this situation have a high surface mobility at the substrate. At higher sputtering pressures, the sputtered atoms are thermalised by the plasma gas, due to the increased number of collisions before arriving at the substrate (Somekh 1984). As a consequence, the sputtered atoms will have a lower surface mobility at the substrate. Therefore, pressure has an important effect in the growth kinetics of the films.

At low argon pressures, the films were found to be under compressive stress, while at higher pressures the stress found to be tensile (Materne et al. 1988). It is understood that at low pressures, the high surface mobility of the sputtered atoms promotes the formation of dense films which are under compressive stress. At higher pressures, the sputtered atoms are less energetic because of the increased scattering. This causes the sputtered atoms to arrive at the substrate at more different angles and results in the films having a columnar morphology, which induces a tensile stress in the film.

Target-Substrate Distance: The distance between the target-substrate has a similar effect with sputtering pressure on the growth kinetics. Increasing the separation has the effect of lowering the mobility of the atoms at the substrate; the reverse is true when the separation is decreased. There is also a close relationship between growth rate and grain size of the films. A low sputtering rate promotes the formation of small grains while a fast sputtering rate results in films with large grain size. Growth rate can be controlled by sputtering power, deposition pressure and target substrate distance.

Sputtering Power: The sputtering power also has the similar effect to that of the pressure as described above. At low powers, the film is in a state of tensile stress, whereas the stress becomes compressive at higher powers. This is due to the increasing kinetic energies of the particles and surface mobility. The deposition rate increases linearly with increasing power but the rate can be increased by use of magnetrons with the target. This produces a denser plasma at the target surface, which increases the deposition rate without increasing the power. However, the use of low sputtering powers causes the system, target and substrate temperature minimized.

Substrate Temperature: The substrate temperature is very important in controlling the properties of the depositing film. It is important that the unintentional substrate heating due to plasma be maintained close to the room temperature. The temperature of the substrate will also influence the surface mobility of the sputtered atoms. The increase in the surface temperature is mainly due to energetic sputtered atoms.

2.2. Magnetic Properties

A material is constructed of atoms, each with a magnetic moment. These magnetic moments come from three sources: the atom's orbital angular momentum, the electron spin and the change in the orbital moment induced by an applied magnetic field. When the field is applied, these magnetic moments tend to either align themselves with the applied field, which is called paramagnetism, or to align in the opposite direction, as in diamagnetism. This alignment of magnetic dipoles caused a net polarization. When a material retains this polarization after the magnetic field is removed, then it is said to be ferromagnetic.

In paramagnetism, when atoms have magnetic moments that interact very weakly with each other, they tend to align themselves with the external field in order to minimize energy. Ferromagnets result from a much stronger interaction between the spin of one atom and that of another close by it. In an applied field, the magnetic moments align with the field, as in a paramagnetic material. The system will prefer a state that minimizes the energy and this requirement aligns the spins and consequently the magnetic moments in the same direction. When the field is removed the material will remain magnetized because of the strong exchange interaction between the spins.

The magnetization, M, is defined to be the magnetic moment per unit volume,

$$M = \frac{m}{V} \ [emu/cm^3]$$

M is a property of the material, and depends on both the individual magnetic moments of the constituent ions, atoms or molecules. The cgs unit of magnetization is the emu/cm^3.

As found in nature, ferromagnetic materials do not have a large net polarization. Instead, there are regions in which magnetic moments are arranged in the same direction, called domains. The separations between these domains are called domain walls. The domain structure also results from a need for the system to minimize energy. In Fig. 2.2(a), a single (mono) domain is shown. In this configuration the magnetic energy will be high due to a large demagnetization contribution. For the case in Fig. 2.2(b) the magnetic energy will be reduced by dividing the sample into two domains which are magnetized in the opposite way. This causes the formation of the domain

walls between the domains. Depending on the magnitude of the exchange interaction and magnetic anisotropy, the energy contained in the domain wall might be so high that domain formation is not favorable. By dividing the crystals into more domains like Fig. 2.2(c) and (d) the demagnetization energy is minimized. The domain structures are often much more complicated. However, domains always lower the energy from a saturated system with high magnetic energy to a domain configuration with lower energy (Andersson 2006).

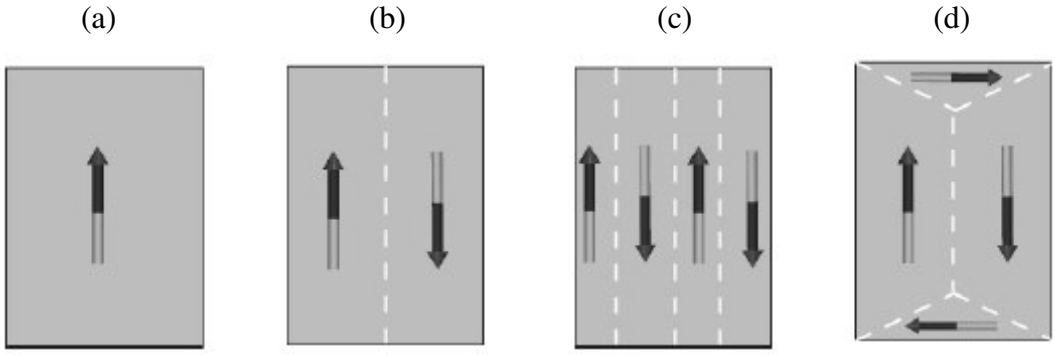

Figure 2.2. The figure shows different domain configurations; (a) a mono domain. (b) a sample with two domains. (c) a sample divided into four domains, and finally (d) closure domains where the demagnetization energy is minimized.

If an external magnetic field is applied to the sample, the number of domain walls shrinks, until a single domain forms. When the applied field is removed, the number of domains increases until the energy to produce a new wall is no longer less than the energy stored in the surrounding fields. It is the domain wall motion that gives the hysteresis in the magnetization, as shown in the Fig. 2.3.

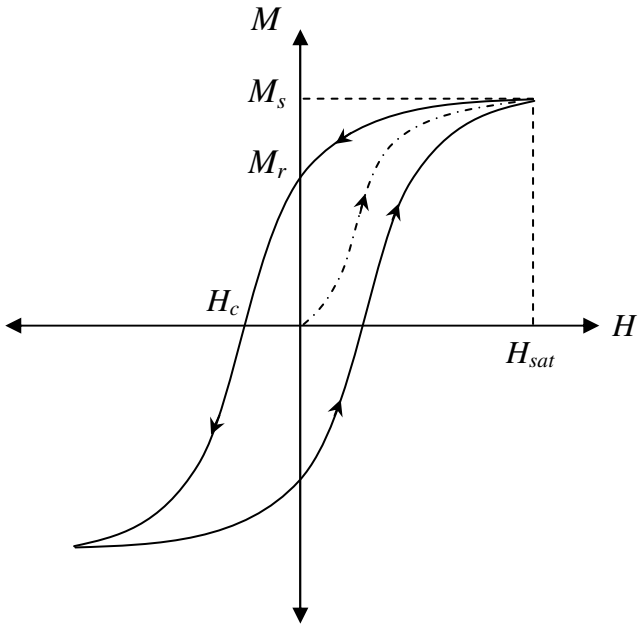

Figure 2.3. A typical hysteresis loop for a ferromagnetic material. The dotted curve shows the initial magnetization curve. Saturation magnetization (M_s), remanence (M_r), and coercivity (H_c) are illustrated on the curve.

To study the graph more carefully several terms must be defined. The distance intersected by the curve on the x-axis is called *coercivity* (H_c) and the field needed to bring the magnetization to zero is called *coercive field*. The lesser the coercivity the more sensitive the material is to the applied field. When the hysteresis loop begins to flatten a condition called *saturation* has been reached with only one domain. At saturation the value of the magnetization is at a maximum called the *saturation magnetization* (M_s). As mentioned, domain motion mainly determines the shape of the hysteresis loop, and is very sensitive to structural properties of the film.

The magnetic properties of films can be affected by structural properties. Saturation magnetization may decrease if any unwanted chemical compound forms during the sputtering process, or if there is intermixing between layers at the interface. Defects in the film tend to increase the coercivity of the hysteresis loops since the domain walls hang on the defects and impurities in the film, making it much more difficult for a single domain form. Therefore, it takes greater applied field to produce a similar effect in a sample containing impurities and defects, limiting the films usefulness as a TMR or GMR device. The roughness of the surface at each interface can also change the magnetic properties. The

rougher the transition between layers the greater the diffuse scattering of electrons. This lowers the changes of a strong GMR or TMR effect.

2.3. Material Properties

2.3.1. Cobalt (Co)

Cobalt is a transition metal and it is a group VIII metal with $3d^7\ 4s^2$ electronic configuration. Cobalt thin film structures have been intensively studied during the last few years because of their possible applications in many areas of technology, such as (i) magnetic data storage devices and sensors; and (ii) spintronics devices where one requires a material which will act as a source of spin polarized electrons. Co plays an important role due to high spin polarization of carriers at the Fermi level (Sharma 2006, Warot-Fonrose 2006).

At ambient pressure bulk Co has two stable phases: HCP (hexagonal close packed) and FCC (face-centered cubic). These structures are shown in Fig. 2.3. The hcp phase is stable below 715 K and fcc phase above that temperature. The bulk resistivity of cobalt is 6.24 μΩ cm. The lattice parameters are $a = b = 2.5071$ Å, $c = 4.0695$ Å for hexagonal structure and $a = 3.5441$ Å for fcc structure. The *c/a* ratio is 1.62 and the magnetization of bulk cobalt is 1422 emu/cm^3 and the ratio of c/a is 1.62 (Bensmina et al. 1999).

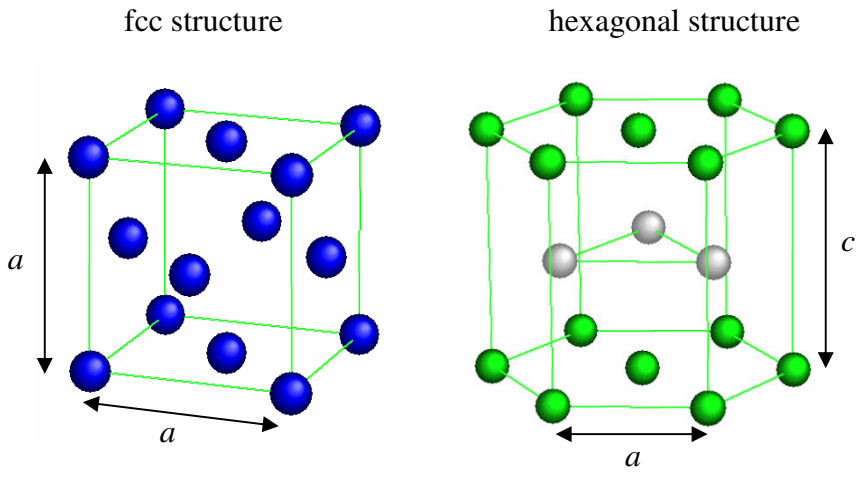

Figure 2.4. The face-centered cubic (fcc) and hexagonal close packed (hcp) structures of Cobalt.

2.3.2. Tantalum (Ta)

Tantalum (Ta) is a group V metal. Because of its low resistivity, Ta films could have important applications in microelectronics such as diffusion barrier and ohmic contacts. It has high melting point and low reactivity so it makes a good capping layer.

The property and crystal structure of tantalum thin films are dependent on the deposition techniques and conditions (Roy 1993, Hoogeveen 1996). Two phases of tantalum can be formed: bcc α-phase and tetragonal β-phase (Fig. 2.4). The latter has an as-deposited resistivity of 170-210 μΩ cm and the former, a good candidate for thin film interconnections and diffusion barriers, has a much lower resistivity of 15-60 μΩ cm (Liu et al. 2001). It is proposed that the lattice parameters of tetragonal tantalum grown on different substrates are $a = b = 10.194$ Å, $a = 5.313$ Å and for bcc tantalum $a = 3.3013$ Å (Read 1965, Jiang 2003, Lee 2004).

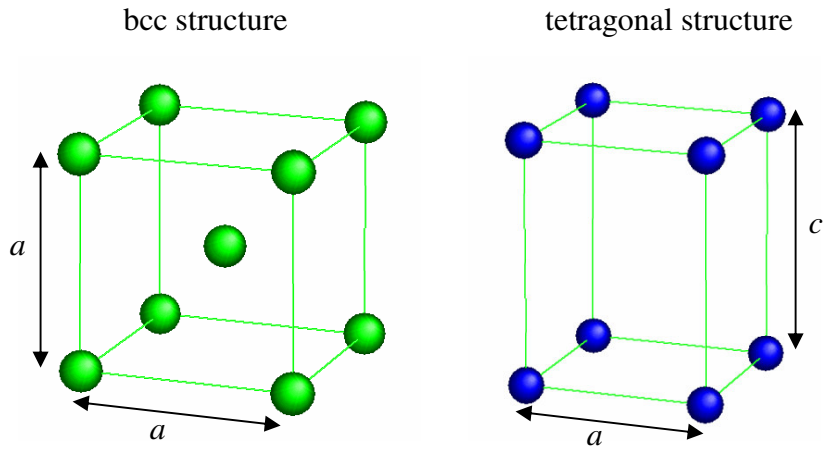

Figure 2.5. The body-centered cubic (bcc) and tetragonal structures of Tantalum.

Tantalum exhibits a wide range of compositions with oxides. Numerous crystalline forms have been identified such as Ta_2O, TaO, TaO_2, Ta_2O_5, and Ta_3O_9. Among these forms, Ta_2O_5 is recognized as the most stable one (Cheng 2003). It has a high dielectric constant (25) and a refractive index of about 2.2 (WEB_2 2007). Thus it can be used as a gate insulator in thin film memory devices (Rao et al. 1999). Band gap of bulk Ta_2O_5 is around 4.2 ev (Demiryont et al. 1985).

In this study, our aim is to grow Ta_2O_5 layer in order to investigate the structure as a barrier layer due to its low band gap and high dielectric constant. Tantalum reacts strongly with silicon to form silicide interface layer which bonds the film strongly to the substrate. Therefore, we deposited tantalum on silicon in order to have well grown cobalt and a good contact layer.

2.3.3. Silicon (Si)

Silicon is widely used in bulk and thin film form in microelectronics applications.

The lattice parameter of silicon is 5.430 Å and it has a diamond fcc structure which is shown in Fig. 2.5. The resistivity of bulk silicon is 0.1 Ω cm. Silicon substrates which have (100) orientation were used in this study.

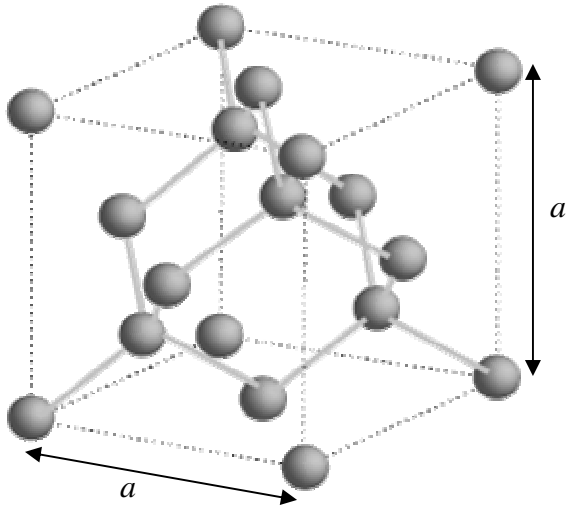

Figure 2.6. Crystal structure of Silicon.

CHAPTER 3

EXPERIMENTAL

This chapter describes the process of magnetron sputtering and the various instruments and methods used for the characterization of the cobalt and tantalum thin films grown in this study. The crystallinity of the films was analyzed by X-Ray Diffractometer (XRD). Surface morphologies and cross-sectional images were investigated by Atomic Force Microscopy (AFM) and Scanning Electron Microscopy (SEM), respectively. Vibrating Sample Magnetometer (VSM) was used to determine magnetic properties of the films.

3.1. Magnetron Sputtering System

The dc sputtering system composed of a pair of electrodes. The cathode is the target material to be deposited. The substrates are placed on the anode. The Ar^+ ions generated in the glow discharge are accelerated at the cathode and sputter the target, resulting in the deposition of the thin films on the substrates.

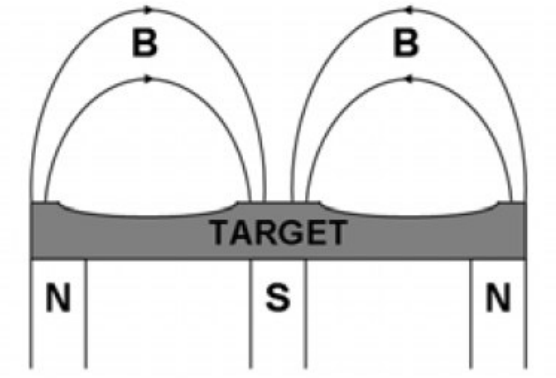

Figure 3.1. Schematic view of the magnetron cross-section and the erosion area formed on the surface of the target.

In magnetron sputtering, a magnetic field is applied on the target surface, as schematically shown in Fig. 3.1. The electrons involved in the sputtering process are trapped in this field close to the target and make cycloidal motion. This electron trapping effect increases the collision rate between the electrons and the sputtering gas molecules.

In this study, the apparatus used to deposit films is ATC Orion 5 UHV Sputtering System (AJA International) in the Department of Physics at Izmir Institute of Technology and shown in Fig. 3.2. This system is a computer-controlled ultra high vacuum system with five 2" magnetron sources. It also consists of a rotating substrate holder (which allows a uniform film deposition) and a sample insertion load-lock chamber.

Figure 3.2. ATC Orion 5 UHV Sputtering System (AJA International) in the Department of Physics at Izmir Institute of Technology.

A halogen lamp based heater above the substrate holder can be used for heating the substrate from room temperature to 850^{o}C as illustrated in Fig. 3.3. The base pressure of about 5 x 10^{-8} Torr is achieved by pumping the system using a turbo pump

backed by a mechanical pump. Both DC and RF sputtering can be done with a maximum power output of 500W and 300W, respectively. Co-deposition of different materials is also possible in this system. The computer control allows us to deposit very thin multilayers with a great accuracy of atomic layer thickness.

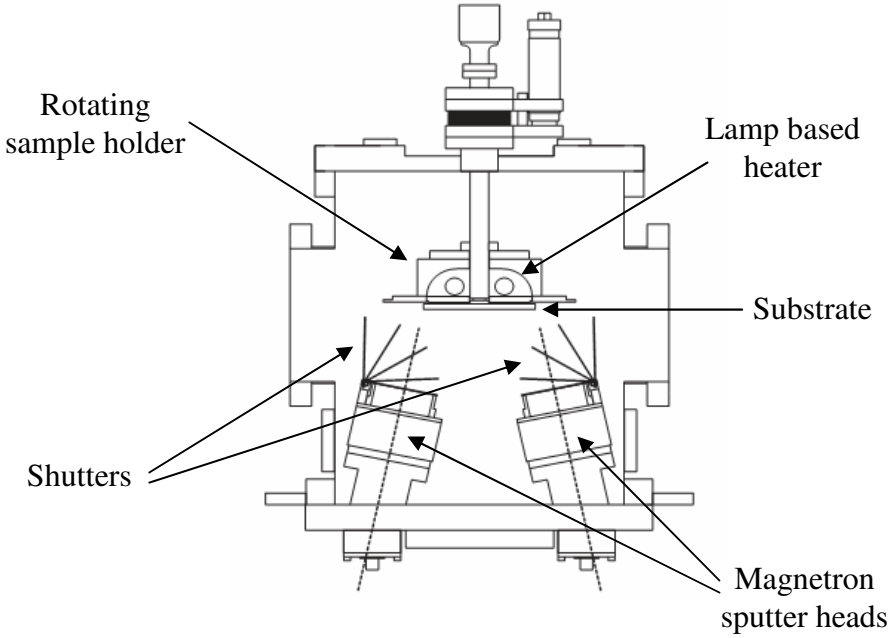

Figure 3.3. Schematic illustration of magnetron sputtering system (AJA International).

3.2. Target and Substrate Preparation

The magnetic thin films were sputter deposited from a 2" cobalt (Co) target with 0.100" thickness and 99.95% purity, a 2" tantalum (Ta) target with 0.250" thickness and 99.95% purity, and a 2" tantalum pent oxide (Ta_2O_5) target with 0.125" thickness and 99.90% purity. The magnet configuration of the magnetron heads were modified for magnetic film deposition.

2" n-type silicon (100) oriented wafers with resistivity 1-10 Ω.cm and 300 μm thickness were used as substrate. In order to have high quality films, substrate should be cleaned properly either chemically or applying a bias voltage to the substrate to etch clean. After cutting the substrates into small pieces (~2x2 cm), they were only cleaned by a stream of dry nitrogen gas to remove any surface dust particles before loading to the system.

3.3. The Deposition Procedure

The substrates were cleaned by RF biasing. Etching the surfaces by RF bias is the preferred method of pre-cleaning since it works with conducting substrates, dielectric substrates and conducting substrates with the deposited insulating films. Substrates were etched for 2 minutes (~10 Å/min) at 15 watts. The targets were always pre-sputtered in order to remove any contamination and oxidation of the surface.

For our system, 12 sccm Ar gas flow corresponding to 3 mTorr of deposition pressure was used for both DC and RF sputtering. Deposition parameters of cobalt, tantalum and tantalum pent oxide films were determined by using Maxtek TM-350 Thickness Monitor. Table 3.1 shows the detailed growth parameters. Both Co and Ta films were deposited using DC sputtering at a power 20W while Ta_2O_5 was grown using RF sputtering power of 15 W at room temperature. Some of the films were then annealed inside the deposition chamber at high vacuum using the substrate heater at 450^{o}C to remove the stresses induced in the film during the deposition. All of the deposited samples are listed in Table 3.2.

Table 3.1. Deposition parameters of Co, Ta and Ta_2O_5 films at different pressures.

Material	**Pressure (mTorr)**	**Power (W)**	**Current (mA)**	**Voltage (V)**	**Rate (Å/min)**
Co	0.5	20	55	350	11.7
	1.3	20	60	324	10.6
	3.0	20	65	296	8.0
	5.0	20	70	278	7.1
Ta	3.0	20	71	271	13.2
Ta_2O_5	3.0	15	11	145	13

Table 3.2. Deposition parameters for all samples.

Sample [Thickness (nm)]	**Power (Watts)**	**Growth Rate (Å/s)**	**Gas Flow (sccm)**	**Pressure (mTorr)**
Si(100)/Co[4]	20	0.2	12	3.0
Si(100)/Co[8]	20	0.2	12	3.0
Si(100)/Co[15]	20	0.2	12	3.0
Si(100)/Co[25]	20	0.2	12	3.0
Si(100)/Co[50]	20	0.2	12	3.0
Si(100)/Co[75]	20	0.2	12	3.0
Si(100)/Co[100]	20	0.2	12	3.0
Si(100)/Ta[40]	20	0.2	12	3.0
Si(100)/Ta[80]	20	0.2	12	3.0
Si(100)/Ta[7]/Co[4]	20 for all	0.2 (Co) 0.2 (Ta)	12 for all	3.0 for all
Si(100)/Ta[4]/Co[25]	20 for all	0.2 (Co) 0.2 (Ta)	12 for all	3.0 for all
Si(100)/Ta[40]/Co[4]	20 for all	0.2 (Co) 0.2 (Ta)	12 for all	3.0 for all
Si(100)/Ta[40]/Co[25]	20 for all	0.2 (Co) 0.2 (Ta)	12 for all	3.0 for all
Si(100)/Ta[7]/Co[4]	20 for all	0.2 (Co) 0.2 (Ta)	5 (Co) 12 (Ta)	0.5 (Co) 3.0 (Ta)
Si(100)/Ta[7]/Co[4]	20 for all	0.2 (Co) 0.2 (Ta)	7 (Co) 12 (Ta)	1.3 (Co) 3.0 (Ta)
Si(100)/Ta[7]/Co[4]	20 for all	0.1 (Co) 0.2 (Ta)	19 (Co) 12 (Ta)	5.0 (Co) 3.0 (Ta)
Si(100)/Ta[40]/Co[25]/Ta[7]/ Co[4]/Ta[7]	20 for all	0.1 (Co) 0.2 (Ta)	12 for all	3.0 for all
Si(100)/Ta[40]/Co[25]/Ta_2O_5[7]/ Co[4]/Ta[7]	20 (Co) 20 (Ta) 15 (Ta_2O_5)	0.1 (Co) 0.2 (Ta) 0.2 (Ta_2O_5)	12 for all	3.0 for all

3.4. Characterization Techniques

3.4.1. X-Ray Diffractometer (XRD)

X-ray diffraction is one of the most common techniques for investigating the structure of crystalline materials. About 95% of all solid materials can be described as crystalline. The basic principle of XRD is the interference of waves reflected from different crystal planes (Cullity and Stock 2001). When an X-ray beam hits an atom, the electrons around the atom start to oscillate with the same frequency as the incoming beam. In almost all directions we will have destructive interference. However, the atoms in a crystal are arranged in a regular pattern, and in a very few directions we will have constructive interference. The waves will be in phase and there will be well defined X-ray beams leaving the sample at various directions (Mohite 2004, WEB_1 2007). From the angle at which constructive interference occurs it is easy to determine the lattice spacing, d, by means of the Bragg law,

$$2d \sin\theta = n\lambda$$

where θ is the angle of incidence relative to the planes, n is an integer and λ is the wavelength of the X-ray. The interplanar distance between planes of atoms is a function of the Miller indices (h,k,l) and the lattice parameter a_l. For cubic, hexagonal and tetragonal structures the interplanar spacing d_{hkl} can be obtained from the following expressions;

Cubic $$\frac{1}{d_{hkl}^2} = \frac{h^2 + k^2 + l^2}{a^2}$$

Hexagonal $$\frac{1}{d_{hkl}^2} = \frac{4}{3}\left(\frac{h^2+hk+l^2}{a^2}\right) + \frac{l^2}{c^2}$$

Tetragonal $$\frac{1}{d_{hkl}^2} = \frac{h^2+k^2}{a^2} + \frac{l^2}{c^2}$$

In the case of amorphous materials, there is distribution of the interplanar spacing because of the random nature of the structure. This leads to much broader peaks in the X-ray diffraction patterns (Ali 1999). Furthermore, by means of Sherrer formula, grain sizes of the crystals in deposited films can be estimated;

$$D = \frac{K\lambda}{\beta \cos\theta}$$

with β the line broadening (full width at half maximum intensity (FWHM) shown in Fig. 3.4.) and K the so-called shape factor, which is usually about 0.9.

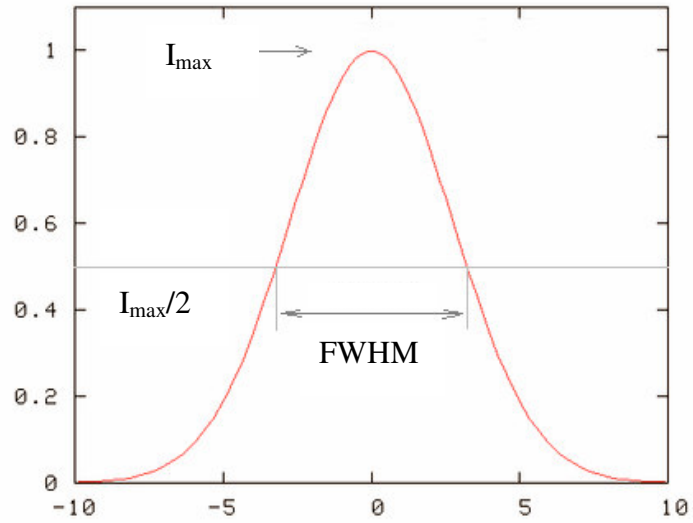

Figure 3.4. Full width at half maximum (FWHM) intensity.

The diffractometer used for the measurements described in this thesis is a Philips X'Pert Pro X-ray diffractometer using a Cu K_α X-ray source. The wavelength of the X-ray is $\lambda_{K\alpha 1}$ = 0.15406 nm. The sample is exposed to the X-rays at an angle θ and reflected rays are detected at an angle 2θ with respect to the original beam.

When the X-rays are incident under a very small angle with the sample surface, the technique is often called grazing incidence X-ray analysis (GIXA) and is very useful for thin film analysis. At these angles reflection of the beam occurs at interfaces. Therefore, film thickness and roughness can be analyzed (Wieldraaijer 2006).

3.4.2. Atomic Force Microscopy (AFM)

Atomic Force Microscopy (AFM) is a useful method for the study of topographic surface features of thin films. AFM is a local surface probing technique. The operation of an AFM is based on the detection of a low power laser beam reflected by the edge of a soft cantilever. The cantilever is typically made of Si as the tip material and oscillates in free air at its resonant frequency. An AFM can operate in principal modes, tapping (non-contact) mode and contact mode. The tapping mode operation is of advantage to investigate the sample surface state without its modification, where as the contact mode is used to add or remove atoms to or from the sample surface.

In this study, an AFM (Multimode SPM, NT-MDT Solver Nova Tech.) with an ultrasharp tip was used in order to perform morphological studies films and roughness measurements of the grown films. AFM was operated in tapping mode.

3.4.3. Scanning Electron Microscopy (SEM)

Scanning electron microscopy (SEM) is a standard method used for characterization of the surface morphology of the thin films. This technique is very useful for a quick view of the entire surface area of a given film. More sensitive methods (e.g. AFM) are slower and allow investigation of only limited area of the sample.

In this thesis, SEM (Phillips XL-30S FEG) was used to analyze the surface and cross-section of the multilayers.

3.4.4. Vibrating Sample Magnetometer (VSM)

Lakeshore 7400 Vibrating Sample Magnetometer (VSM) was used to record the hysteresis loops of Co layers. The electromagnet in the VSM produces a uniform magnetic field between the poles, around the sample, which creates a magnetization in the film. Then, it is allowed vibrate in sinusoidal manner. The changes in flux caused by the vibrations are translated into a change in current in the pickup coils of the instrument, which means as a particular magnetization of the film. With a sensitivity of

10^{-6} emu the VSM gives an accurate measurement of magnetization. A picture of our VSM system can be seen in Fig. 3.5.

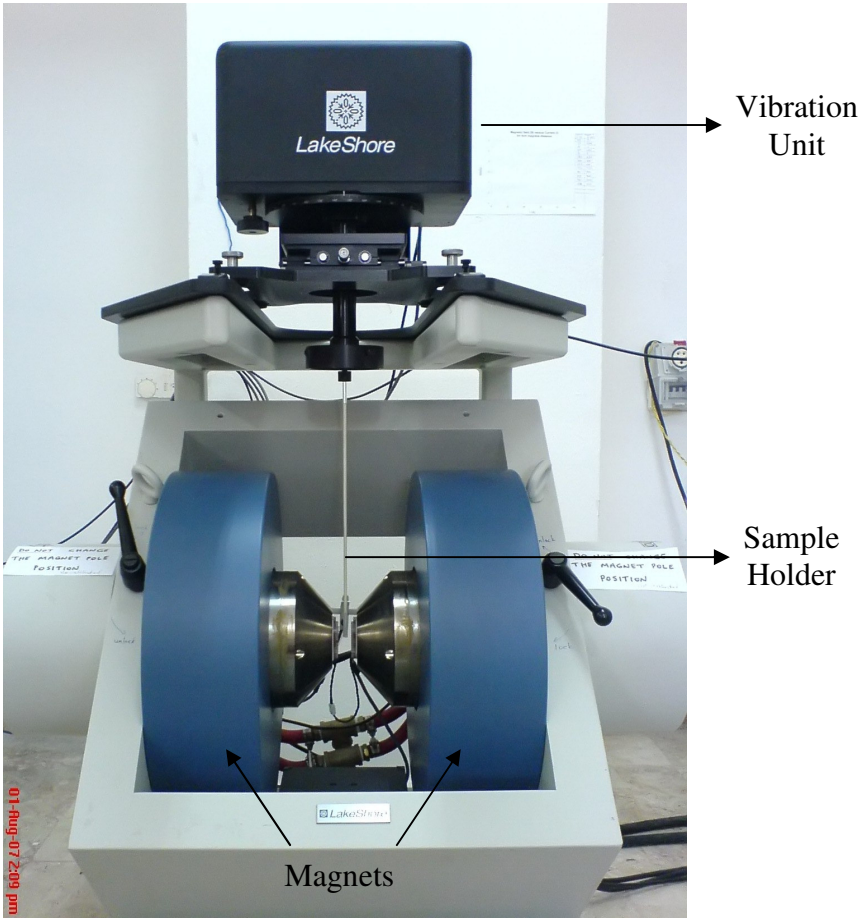

Figure 3.5. Lakeshore 7400 VSM system.

CHAPTER 4

RESULTS AND DISCUSSION

In this chapter, the results of structural and magnetic characterizations of single and multilayers of Ta and Co films will be presented in detail. The growth conditions and parameters for further MTJ structures will be determined in the light of results of this study.

4.1. X-Ray Diffractometer Results

Si/Co:

Fig. 4.1 shows the XRD pattern of Co thin film as a function of film thickness. There is no peak up to 25 nm Co thickness indicating that the film is amorphous. However, XRD pattern recorded on 50, 75, and 100 nm thick Co film shows the signature of crystalline through hexagonal (hcp) structure. The increase in sharpness indicates the increase in grain size of Co thin film. The grain sizes are calculated by using Scherer formula as 15.3, 17.4, and 20.4 nm, respectively. For 100 nm thin film sample one can clearly see an intense peak at $2\theta = 44.53^0$ corresponding to (002) hcp Co. There are also less intense peaks at 41.68^0 and 47.41^0 due to the reflections from (100) and (101) planes, respectively.

In order to investigate the effect of annealing on amorphous structure, we annealed 25 nm Co film at 450^0C in our sputtering chamber for 30 minutes at high vacuum. The XRD scan of as-deposited and annealed films is shown in Fig. 4.2 (a) and (b), respectively. It clearly shows transformation from amorphous to crystalline hcp (002) phase at $2\theta = 44.75^0$ (Kumar and Gupta 2007). There is no other diffraction peak related to other orientations of Co in the spectrum (b) indicating that Co film is single crystal with 0.317 FWHM values and has average grain size of 27 nm. One can infer from this spectrum that the reason of increasing crystallinity is due to disappearing of various point defects and release of stresses. In this sample Co crystallize in the hcp structure and have the <1000> texture. The (200), (222), and (400) peaks for silicon also appears at $2\theta = 32.95^0$, 61.65^0 and 69.10^0, respectively.

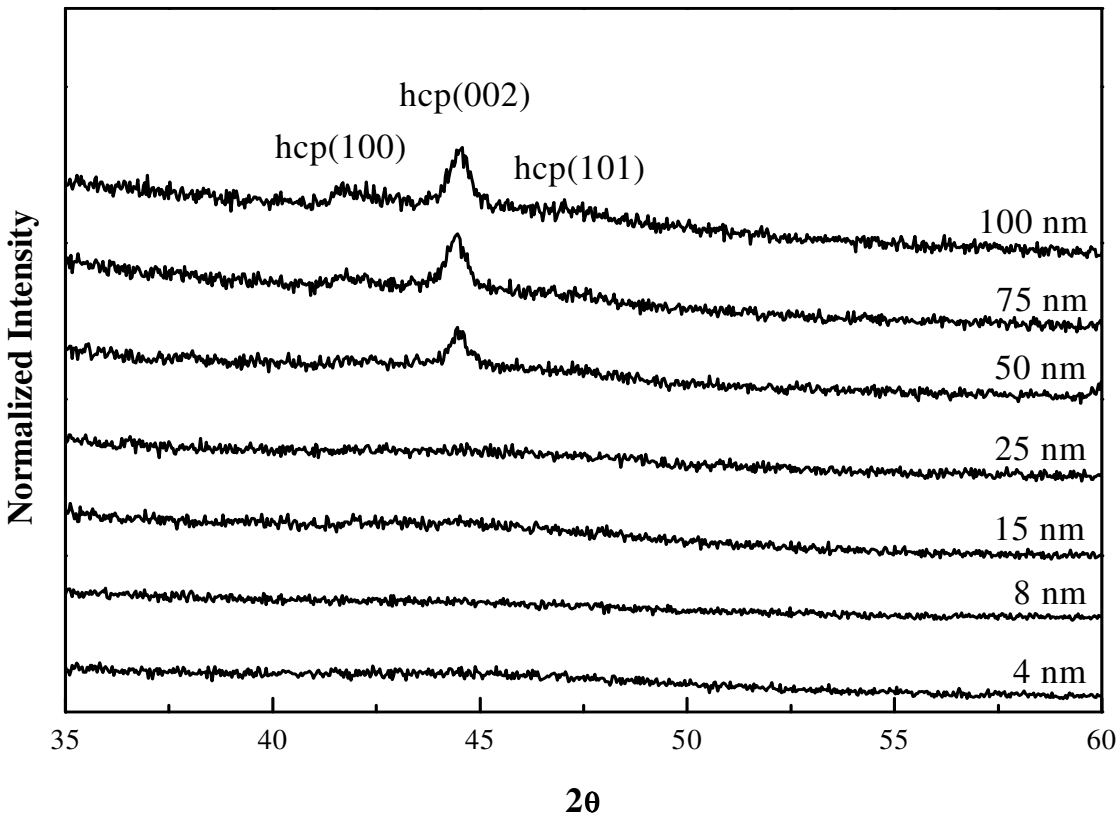

Figure. 4.1. XRD patterns of Co films as a function of thickness.

This amorphous nature of as-deposited film can be due to the structural differences between Si and Co. However, after a critical thickness, Co constructs its own natural hexagonal structure and becomes crystal. The amorphous nature of Co film at lower thickness is also reported in the literature (Sharma 2007, Kharmouche 2004).

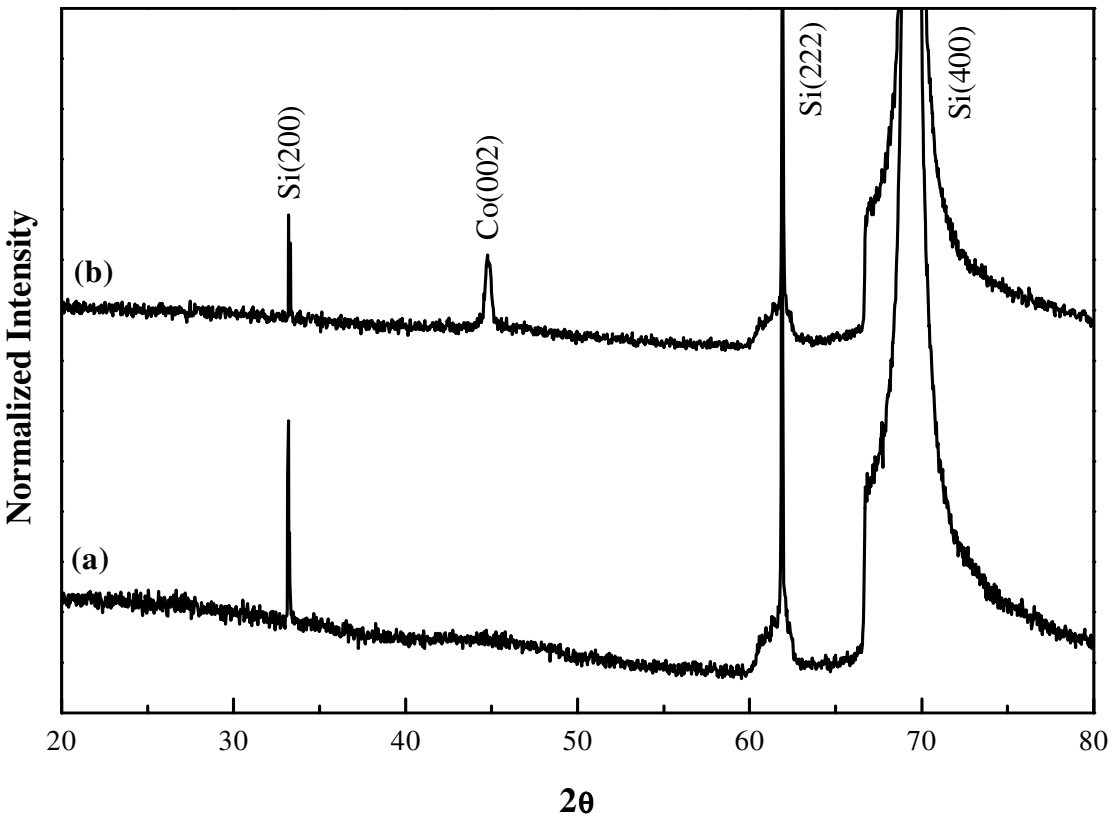

Figure 4.2. XRD patterns of (a) as-deposited and (b) annealed at 450^0C Co film with 25 nm thickness.

Si/Ta:

XRD spectra for room temperature Ta growth on Si(100) with 40 nm thickness is shown in Fig. 4.3. The pattern indicated the presence of single crystalline tetragonal Ta phase (β-Ta) with the orientation along (002) (Kohli 2004, Maeng 2006). The diffraction peak for (002) plane which is at $2\theta = 33.98^0$ shows the presence of strong texture in this Ta film. According to Bragg Law and interplanar spacing formulas, the lattice parameters are calculated to be $a = b = 11.704$ Å and $c = 5.272$ Å. These values are close the international diffraction database for beta tantalum (Lee 2004).

The peak has a value of 0.398 for FWHM and the grain size was calculated as about 21 nm. The reason of this low FWHM value might be because of the low lattice mismatch (6.13%) between β-tantalum and silicon lattice constants. β-tantalum has tetragonal structure and silicon has fcc structure. The structure of deposited film on the

substrate and low lattice mismatch can be seen from Fig. 4.4. Therefore, Ta grows well on silicon and has a very good crystal quality.

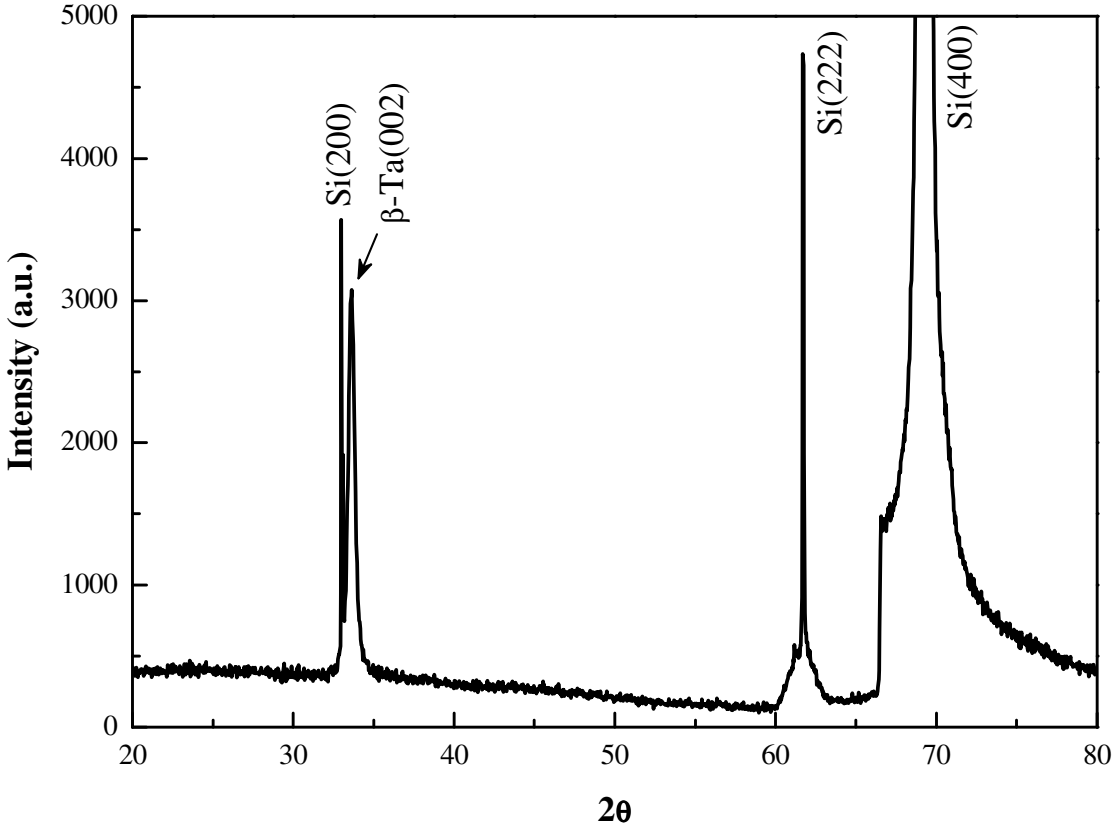

Figure 4.3. XRD spectra for as-deposited Ta on Si(100) with 40 nm thickness.

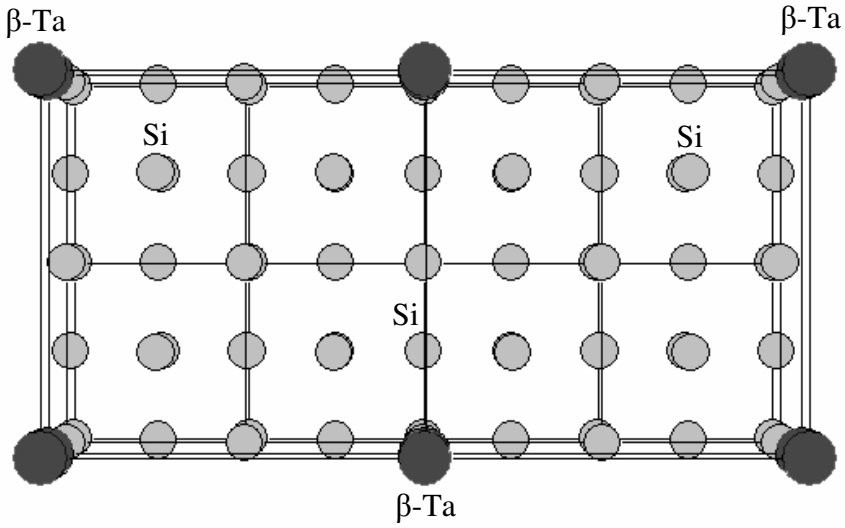

Figure 4.4. The top view image of Ta atoms grown on Si atoms.

Si/Ta/Co:

After analyzing single layers of Co and Ta, Ta/Co bilayers were grown on Si(100) substrate. Fig. 4.5 (a) and (b) show XRD patterns of as-deposited and annealed Si/Ta(7nm)/Co(25nm) bilayer. In the as-deposited pattern, there is no Ta peak because Ta layer is very thin in this sample. As indicated before, there was no peak in Si/Co(25nm) sample. However, when a thin Ta layer is deposited under Co layer, a sharp Co (002) peak appears at $2\theta = 44.65^0$ and it has FWHM value of 0.570 and 15 nm grain size. It can be inferred that Ta buffer layer changes the structure of Co film dramatically. We also annealed this sample at 450^0C for 30 minutes at high vacuum and the XRD scan can be seen in Fig. 4.5 (b). It is seen that the crystallinity of Co increases because the Co peak is sharper and has higher intensity. The grain size increased from 15 nm to 18 nm as well.

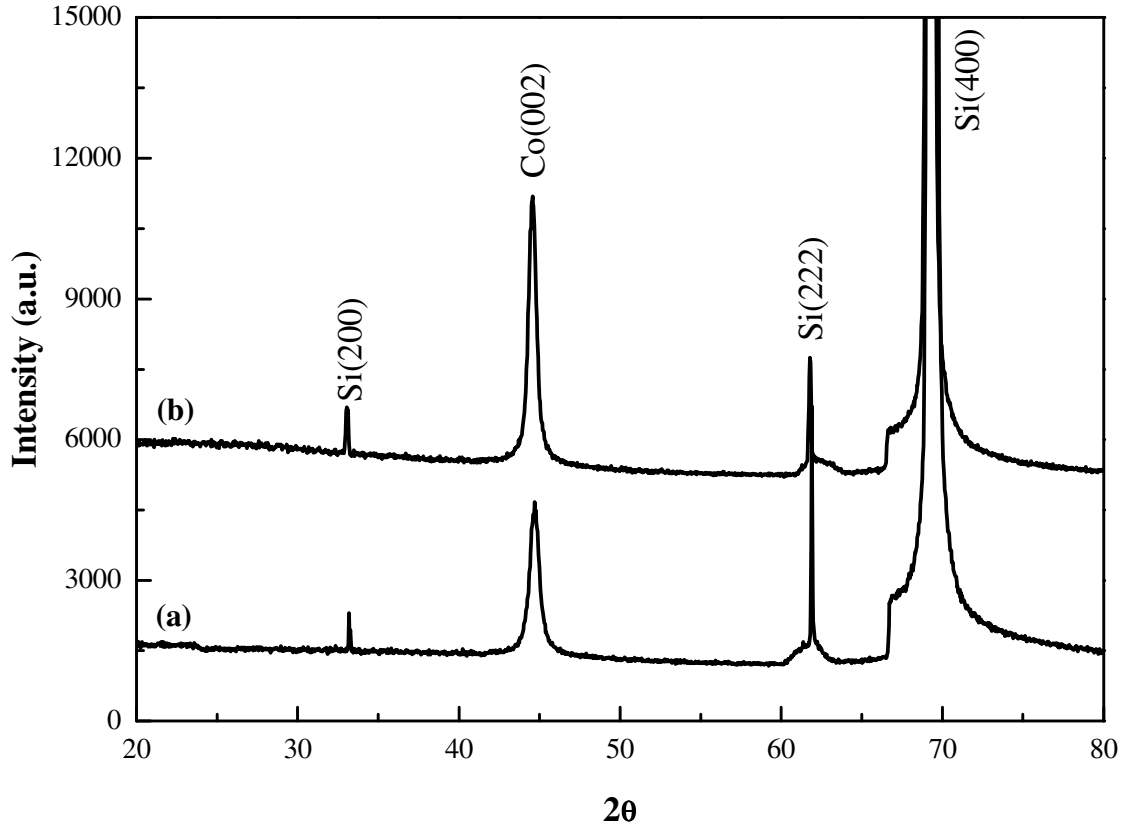

Figure 4.5. XRD patterns of (a) as-deposited and (b) annealed at 450^0C Si/Ta(7 nm)/Co(25 nm) bilayer.

Fig. 4.6 (a) and (b) show the XRD patterns of the as-deposited and annealed samples where Ta thickness was increased from 7 nm to 40 nm for the same bilayer. It is clear that tetragonal β-Ta (002) peak appears at $2\theta = 33.97^0$ and we have hcp Co (002) peak again at $2\theta = 44.65^0$ for both patterns. In spectra (a), Ta and Co peaks are quite sharp with FWHM of 0.400 and 0.649 and grain sizes of 21 nm and 13 nm, respectively. After annealing, Co has better crystallinity again but there is no significant change in the crystallinity of Ta. The FWHM values and the grain sizes can be compared from Table 4.1. One can infer from these graphs that annealing causes better crystallinity for Co films but not for Ta films. This might be the result of defects in cobalt which are disappearing during the annealing process.

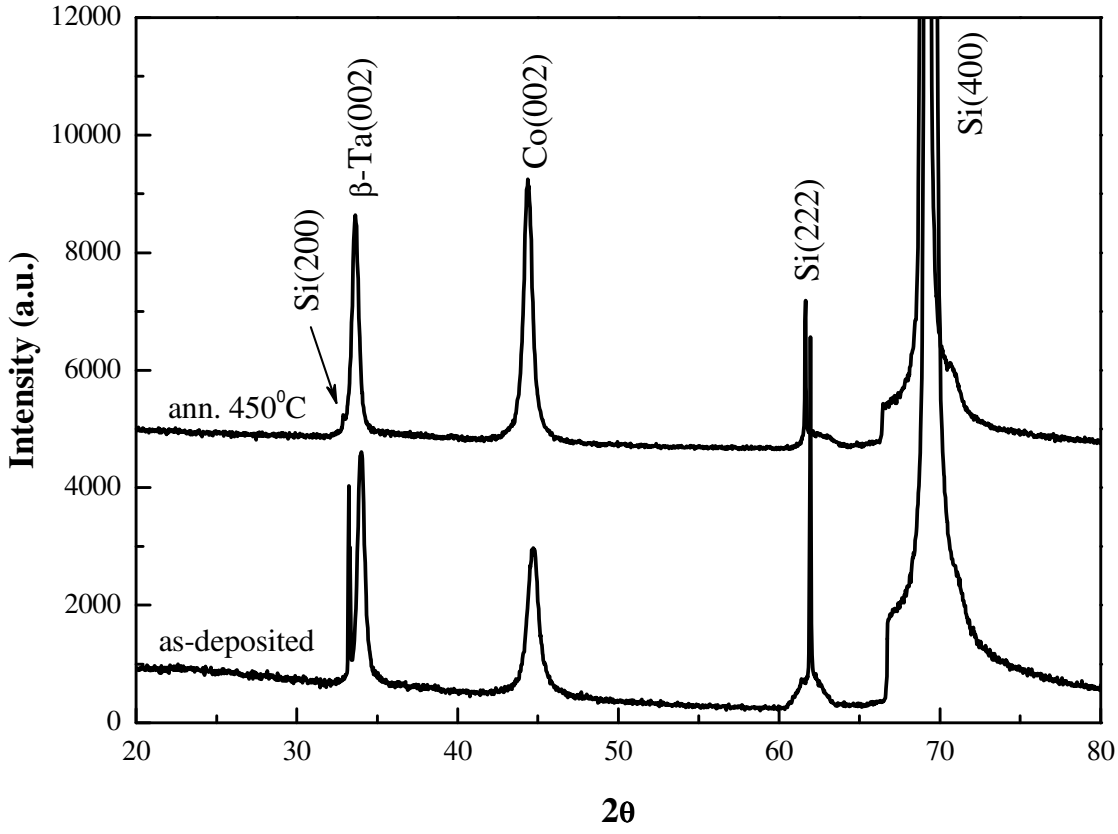

Figure 4.6. XRD patterns of (a) as-deposited and (b) annealed at 450^0C Si/Ta(40 nm)/Co(25 nm) bilayer.

Si/Ta/Co/Ta/Co/Ta:

In order to investigate MTJ structures we need to grow multilayers including two ferromagnetic layers separated by the insulating layer. Before growing TaO_x layer, we deposited Ta spacer layer to see the difference with the oxide layer. Therefore, we deposited Si/Ta(40nm)/Co(25nm)/Ta(7nm)/Co(4nm)/Ta(7nm) and the XRD spectra is shown in Fig. 4.7. Here it can be obviously seen β-Ta (002) and Co (002) peaks similar to Si/Ta/Co bilayers as expected. Tantalum exhibited a good single crystalline quality with FWHM of 0.386 and a grain size of 21.5 nm. Cobalt also has good crystallinity with FWHM value of 0.672 and grain size of 12.8 nm.

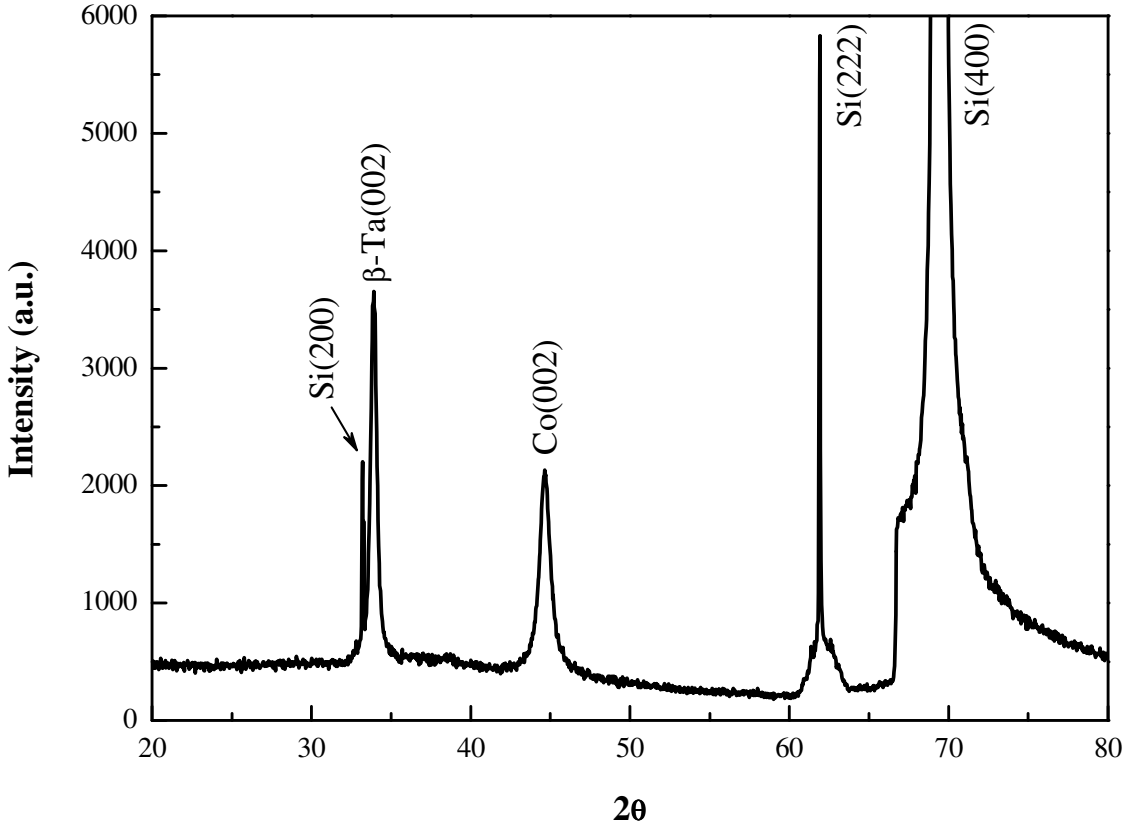

Figure 4.7. XRD spectra of Si/Ta(40nm)/Co(25nm)/Ta(7nm)/Co(4nm)/Ta(7nm).

Si/Ta/Co/Ta_2O_5/Co/Ta:

Having the insulator layer by using Ta_2O_5 target, Si/Ta(40nm)/Co(25nm)/Ta_2O_5 (7nm)/Co(4nm)/Ta(7nm) multilayer was deposited. The XRD pattern of this multilayer is shown in Fig. 4.8. Comparing the previous structure, Ta_2O_5 layer did not make any difference about the crystallinity of Ta and Co layers. Both of them have good crystal quality again. Tantalum has the FWHM value of 0.410 and 20.2 nm grain size. Calculations for Co peak whose intensity seems to be increased showed that the FWHM value of 0.629 and grain size of 13.60 nm. These Co values show better crystallinity than the multilayer where Ta spacer layer is used instead of Ta_2O_5. It can be inferred that Co still keeps the same hexagonal structure when grown on Ta_2O_5 layer and it contributes to the Co (002) peak. All FHWM and grain size values of the single layers, bilayers and multilayers can be found in Table 4.1.

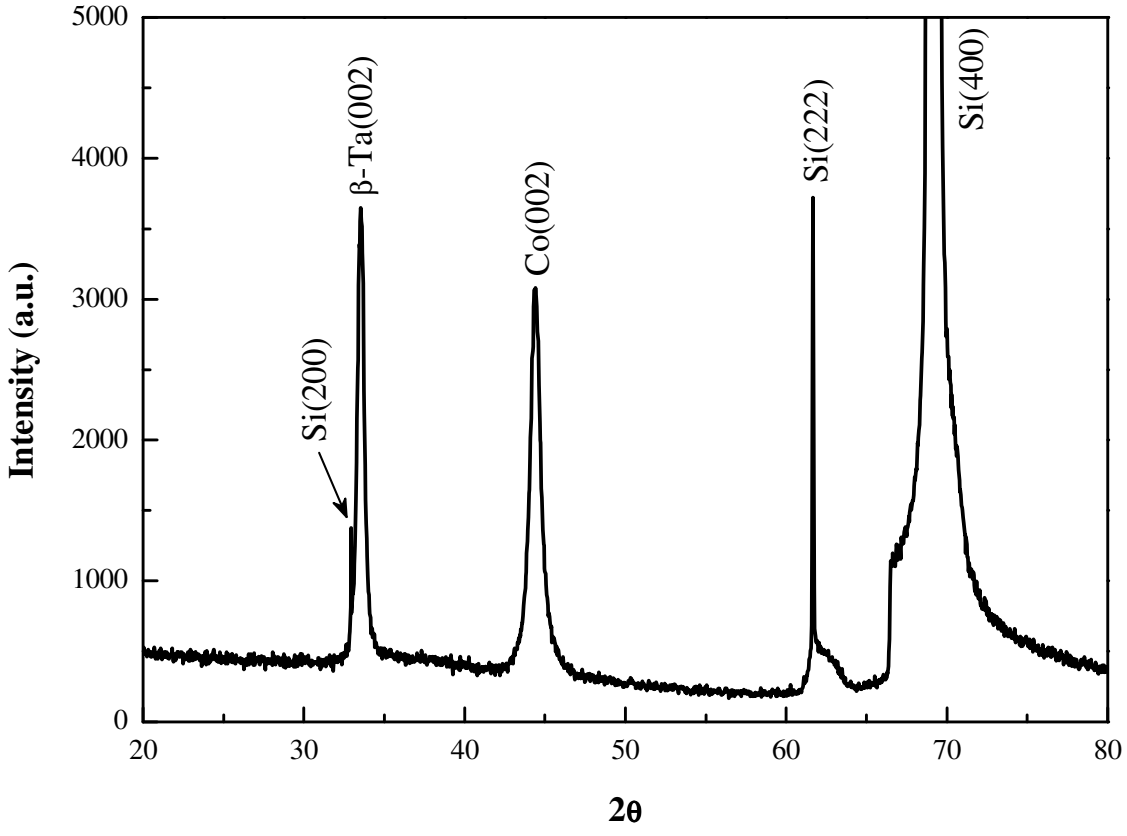

Figure 4.8. XRD diffraction pattern for Ta(40nm)/Co(25nm)/Ta_2O_5(4nm)/Co(4nm)/ Ta(7nm) multilayer on Si(100) substrate.

Table 4.1. FWHM values of diffraction peaks and grain sizes of cobalt and tantalum in single layers, Si/Ta/Co samples and multilayers, respectively and FWHM and grain size for silicon substrate.

Layers	FWHM (Degree)		Grain Size (nm)	
	Co (002)	**β-Ta (002)**	**Co (002)**	**β-Ta (002)**
Si/Co(25) annealed	0,317	-	27.1	-
Si/Ta(40)	-	0.398	-	21.2
Si/Ta(7)/Co(25)	0.570	no peak	15.1	no peak
Si/Ta(7)/Co(25) annealed	0.466	no peak	18.4	no peak
Si/Ta(40)/Co(25)	0.649	0.400	13.2	20.8
Si/Ta(40)/Co(25) annealed	0.508	0.409	16.9	20.3
Si/Ta(40)/Co(25)/Ta(7)/Co(4)/Ta(7)	0.672	0.386	12.8	21.5
Si/Ta(40)/Co(25)/Ta_2O_5(4)/Co(4)/Ta(7)	0.629	0.410	13.6	20.2
Silicon substrate	0.088		109.7	

4.2. Atomic Force Microscopy Results

For the investigation of growth morphology of the as-deposited films, two and three-dimensional AFM images were recorded. All surface images were taken for 3x3 μm^2 areas. Root mean square (rms) roughness values for all samples are summarized in Table 4.2.

The silicon substrate has 1.6 Å surface roughness shown in Fig. 4.9. It is indicating that Si(100) has very smooth surface. Grain sizes of the substrate were found to be ~110 nm from the XRD analysis.

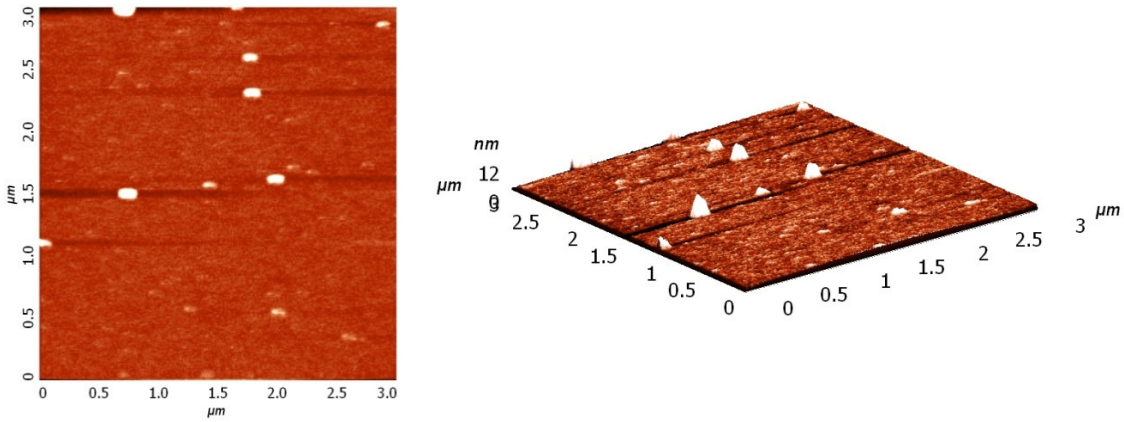

Figure 4.9. AFM images of Si(100) substrate. Roughness (rms) is ~1.6 Å.

Surface morphologies of the Co films on silicon with thicknesses of 4, 15, and 100 nm are shown in Fig. 4.10 - 4.12, respectively. Analyzing the roughness values for various thicknesses, it can be inferred that Co films have smooth and uniform surface structure on silicon. Comparing from the images and Table 4.2, as the thickness increases, surface rms roughness first increases and then decreases. Our Co films were amorphous up to 50 nm and with increasing film thickness, the defects on the film surface can result in roughness increasing slowly until crystallinity starts. After Co starts crystallizing, the grain sizes increase and stress in the film releases so that the surface becomes smoother and continuous with low roughness values. The variation of roughness as a function of Co thickness can be seen in Fig. 4.13.

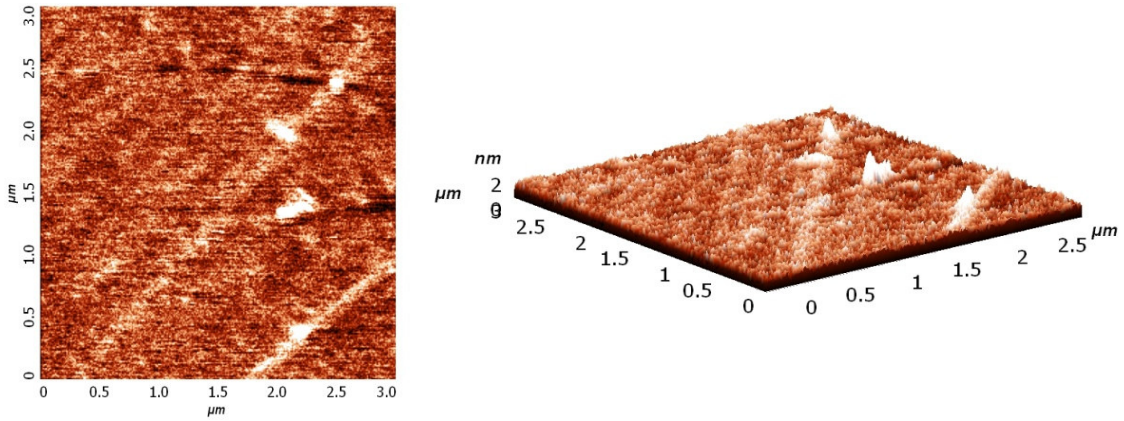

Figure 4.10. AFM images of Si/Co(4nm) thin film. Roughness (rms) is ~1.6 Å.

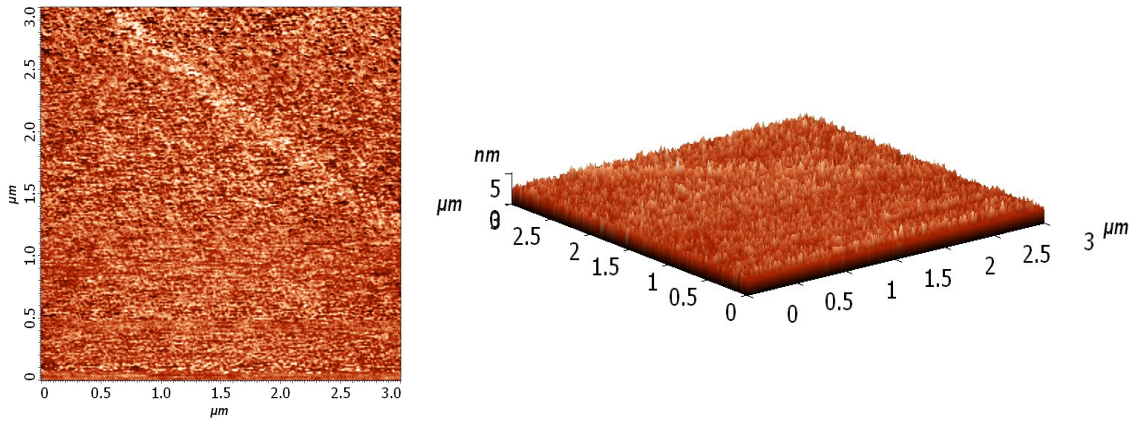

Figure 4.11. AFM images of Si/Co(15nm) thin film. Roughness (rms) is ~5.6 Å.

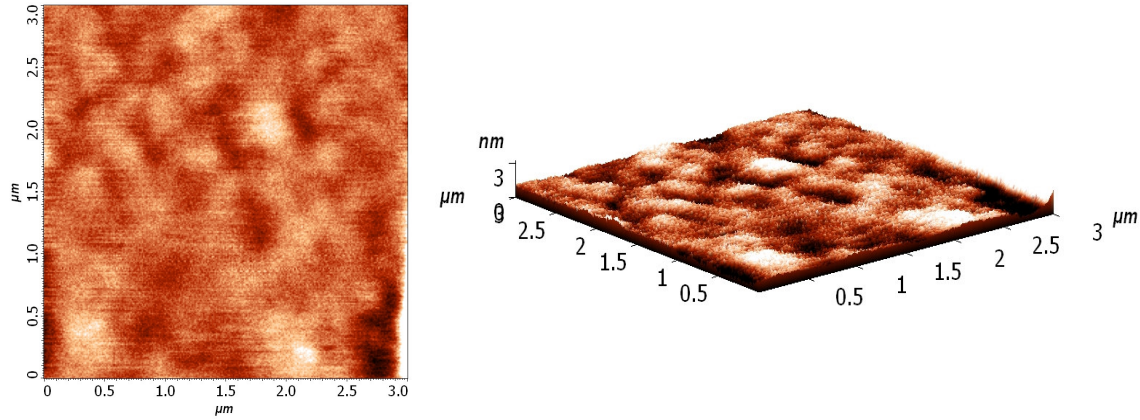

Figure 4.12. AFM images of Si/Co(25nm). Roughness (rms) is ~5.0 Å.

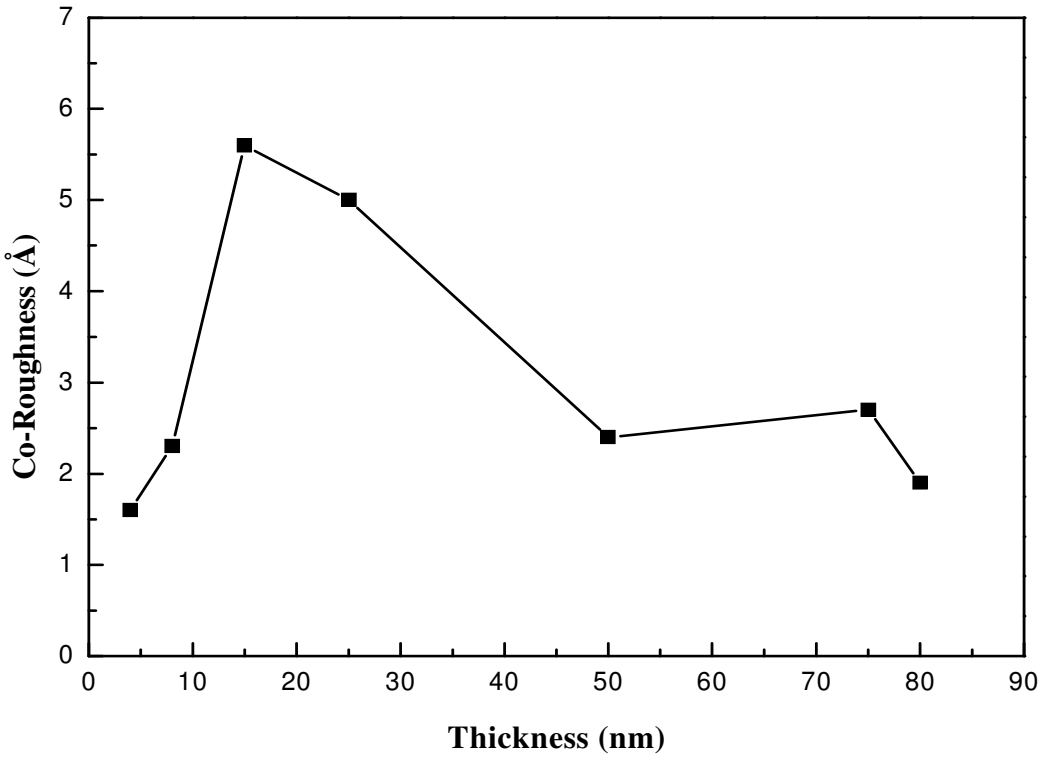

Figure 4.13. Variation of roughness as a function of Co thickness.

Fig. 4.14 and 4.15 show the surface morphologies of deposited tantalum layers on Si(100) substrate. 40 nm Ta film has 0.9 Å surface roughness value which is quite low and smoother than Si substrate. With increasing Ta thickness from 40 to 80 nm, the roughness increased from 0.9 to 2.2 Å. These surface roughness values are good for FM layer to be grown on Ta. Homogeneous and continuous tantalum films are obtained. The reason of having high quality Ta film also might be because of the low lattice mismatch (6.13%) between β-tantalum and silicon substrate.

Fig. 4.16 shows surface roughness measurement for Si/Ta(7nm)/Co(4nm) bilayer. Root-mean-square roughness for this sample was found to be 2.0 Å and this is a quite low value for surface roughness. However, 4 nm Co film on silicon has 1.6 Å roughness value and this shows us that thin Ta layer increases the Co surface roughness slightly.

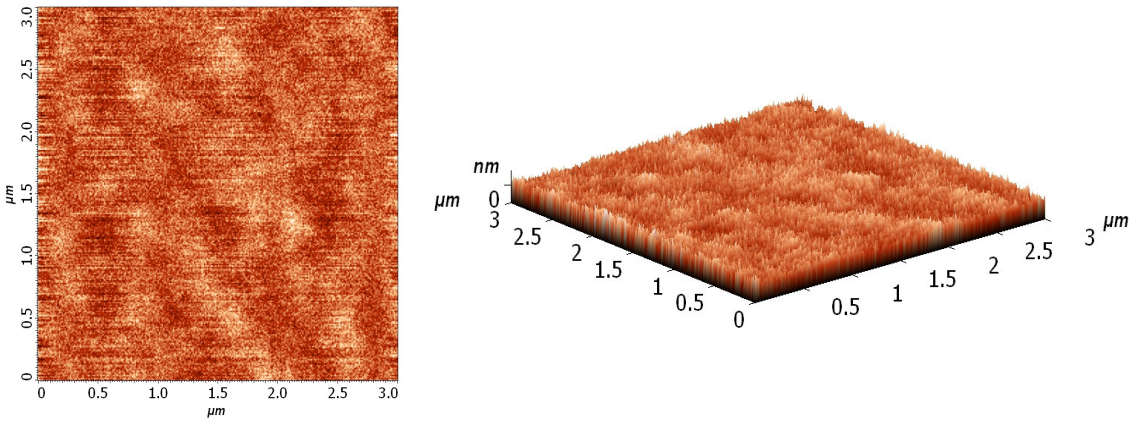

Figure 4.14. AFM images of Si/Ta(40nm) thin film. Roughness (rms) is ~0.9 Å.

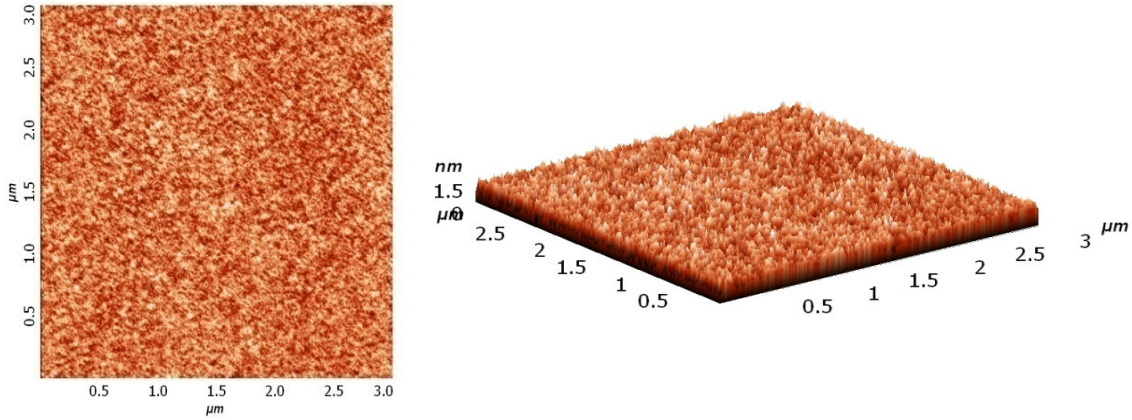

Figure 4.15. AFM images of Si/Ta(80nm) thin film. Roughness (rms) is ~2.2 Å.

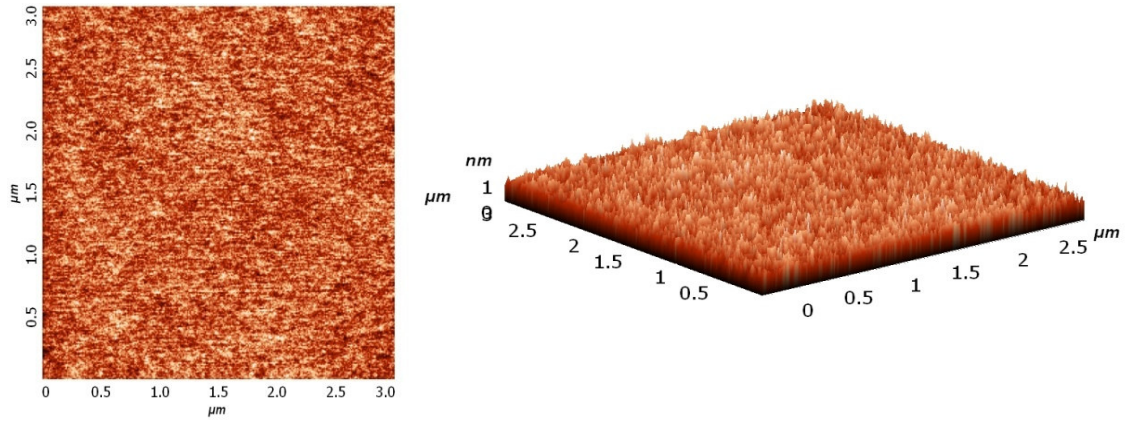

Figure 4.16. AFM images of Si/Ta(7nm)/Co(4nm). Roughness (rms) is ~2.0 Å.

When we increase the Co layer thickness from 4 nm to 25 nm for the same structure, roughness analysis gave us the images shown in Fig. 4.17 which is for Si/Ta(7nm)/Co(25nm). From the obtained surface images, rms roughness was found to be 1.3 Å which is interesting and lower than the previous structure with thin Co layer. Previously, increasing Co film thickness on silicon substrate caused higher roughness value but now thick Co on thin Ta gave us low roughness. As we have found from the XRD measurement of this structure that increasing Co film thickness on thin Ta layer results in single crystal hcp Co structure. Therefore, as the thickness of Co increases, grain size increases which is the reason of good crystallinity of Co, low roughness value and smoother surface.

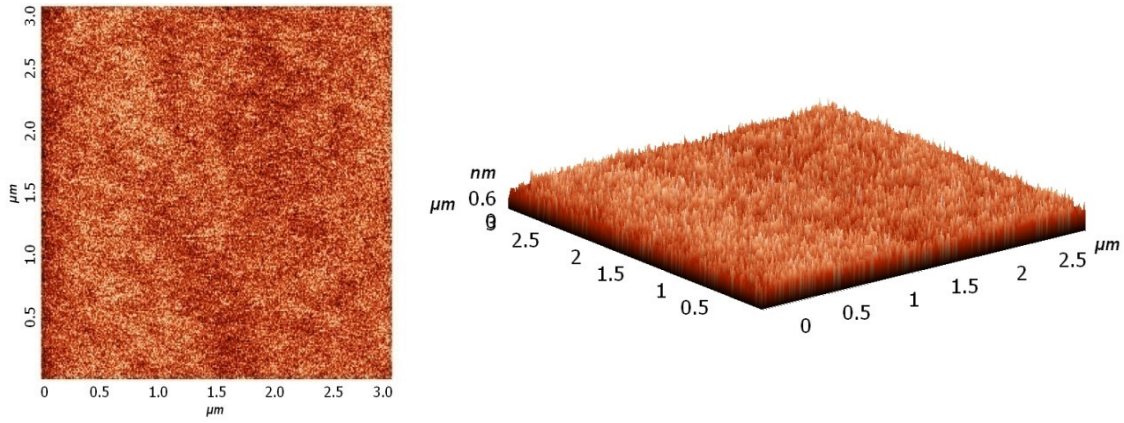

Figure 4.17. AFM images of Si/Ta(7nm)/Co(25nm). Roughness (rms) is ~1.3 Å.

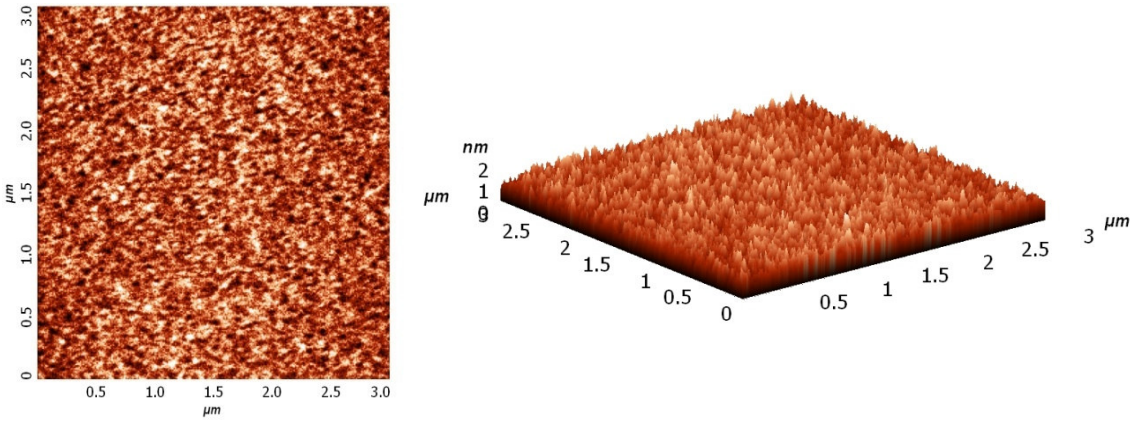

Figure 4.18. AFM images of Si/Ta(40nm)/Co(25nm). Roughness (rms) is ~2.4 Å.

Finally, we also increased Ta thickness for the same layers and obtained AFM images of Si/Ta(40nm)/Co(25nm) which is shown in Fig. 4.18. The roughness value was found to be 2.4 Å for this sample. Comparing with the 40 and 80 nm single Ta layer roughness values, increasing Ta layer thickness causes rougher interface and so rougher Co surface. However, the surface is still uniform and continuous because Co grows single crystal on Ta and large grain size lowers the surface roughness value. These thickness and roughness values are convenient in order to use bottom Ta layer as a contact layer in MTJ structures. In addition, the change in coercivity of Co films is related to the changes in surface roughness. In the case of rough films, the local surface roughness will induce in-plane magnetic poles, which may result in an in-plane demagnetizing field (Tiusan et al. 2002). Surface roughness induced magnetic anisotropy will change the domain size of Co films, thereby inducing the domain wall pinning. A decrease in freedom in domain wall motion thus leads to the enhancement of coercivity (Ng et al. 2002).

Table 4.2. Root-mean-square roughness values for Si substrate, Co, Ta and Ta/Co bilayers.

Samples	**Roughness (Å) [rms]**
Si(100) substrate	1.6
Si/Co(4 nm)	1.6
Si/Co(8 nm)	2.3
Si/Co(15 nm)	5.6
Si/Co(25 nm)	5.0
Si/Co(50 nm)	2.4
Si/Co(75 nm)	2.7
Si/Co(100 nm)	1.9
Si/Ta(40 nm)	0.9
Si/Ta(80 nm)	2.2
Si/Ta(7 nm)/Co(4 nm)	2.0
Si/Ta(7 nm)/Co(25 nm)	1.3
Si/Ta(40 nm)/Co(25 nm)	2.4

4.3. Scanning Electron Microscopy Results

SEM cross-section image of Co(100nm) on silicon substrate is illustrated in Fig. 4.19. Uniform cobalt film layer and continuous deposition can easily be seen from the micrograph. The as-deposited cobalt film consists of very fine columnar structure. Thickness of the cobalt layer was found to be 100 nm for 120 minutes deposition from this micrograph. Intermixing at the interface cannot be commented at this scale.

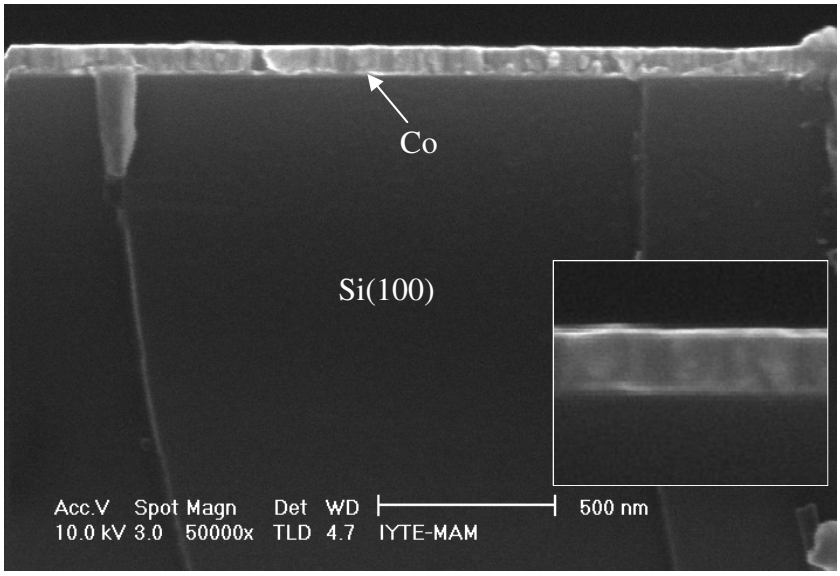

Figure 4.19. SEM cross-section micrograph of Co(100nm) on Si(001).

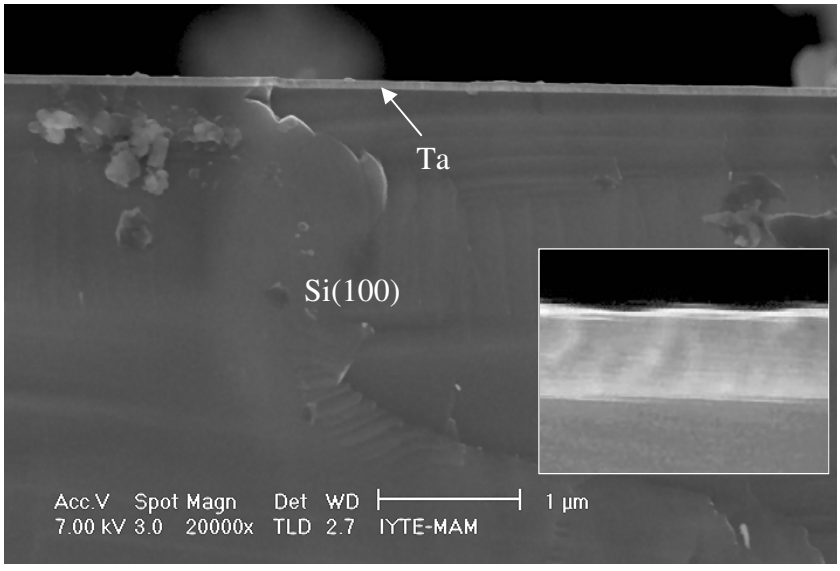

Figure 4.20. SEM cross-section micrograph of Si/Ta(80nm).

Fig. 4.20 shows cross-section of Ta(80nm) single layer on silicon substrate. We have uniform and homogenous film. Thickness of tantalum single layer was found to be 80 nm from this figure for 60 minutes growth.

Fig. 4.21 shows the SEM cross-section image of thick Si/Ta(40nm)/Co(25nm) bilayer. The layers can be easily observed from the image. This film also seems to be uniform and the interface of the top layers can be clearly seen. The thicknesses also show the expected values.

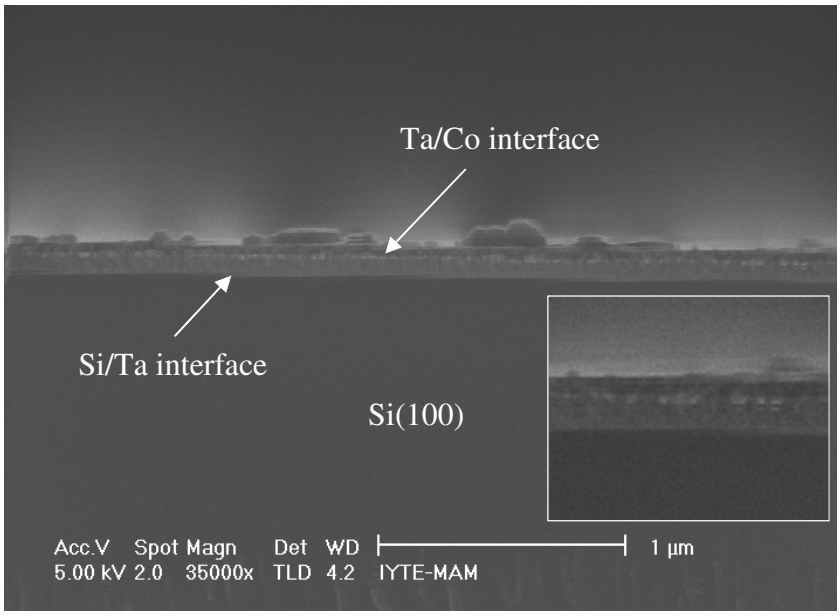

Figure 4.21. SEM cross-section micrograph of Si/Ta(40nm)/Co(25nm).

4.4. Vibrating Sample Magnetometer Results

Hysteresis loops of the samples of various thickness and pressure were measured by VSM. The hysteresis loops allowed us to determine two important parameters: the coercivity (H_c) of the sample, and saturation magnetization (M_s).

The H_c was determined by measuring on the graphs where the magnetization returned to zero after saturation. Hysteresis loops were recorded up to the saturation magnetization. The magnetizations were determined as emu/cm^3. The volume was calculated by measuring the area of the films with a digital caliper multiplying with the thickness of the film.

Co film with thickness of 25 nm on silicon substrate has a square loop for the field applied parallel to the film plane. The directions of easy axis and hard axis in the

film plane were determined from the azimuthal angle dependence of the loop shape (Wu et al. 2001). This suggests an in-plane easy axis for Co films. The hysteresis curves are illustrated in Fig. 4.22 where parallel and perpendicular *M-H* curves for the 25 nm thick Co film are shown.

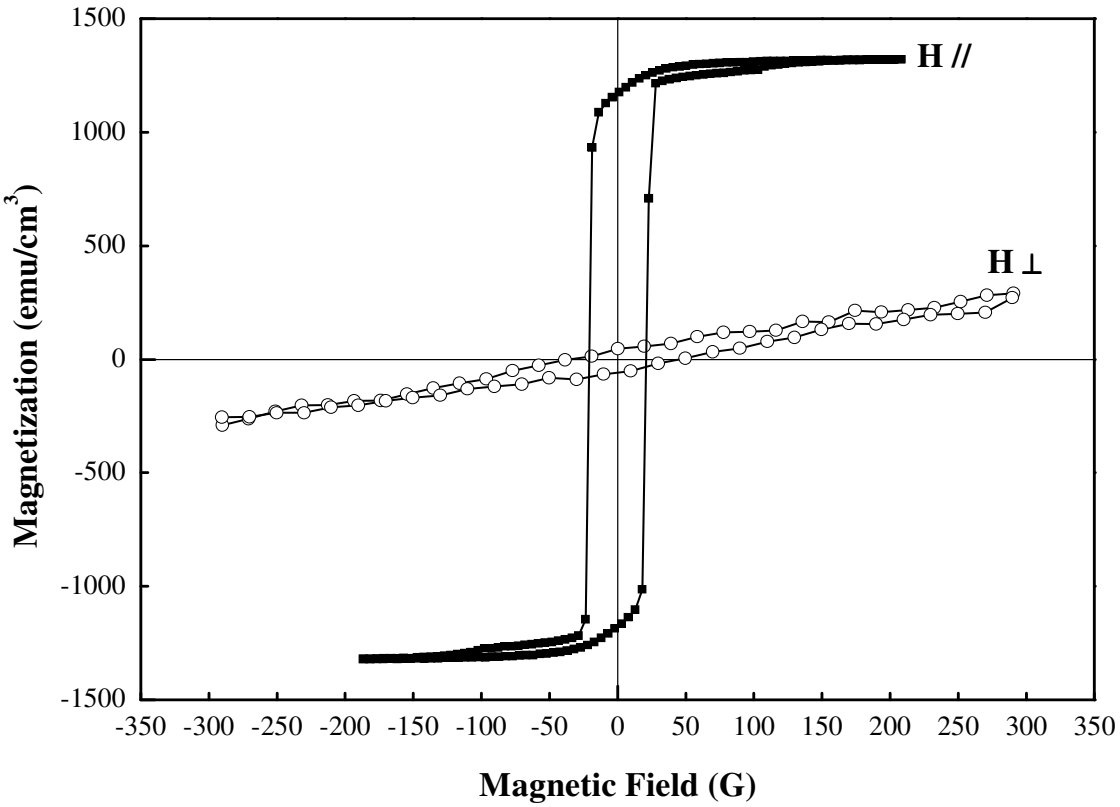

Figure 4.22. Hysteresis curves of Si/Co(25nm) film with applied field parallel and perpendicular to the film plane.

The loop had a square like shape, low H_c about 20 gauss and a high squareness S about 0.88 when the magnetic field was applied parallel to the film plane. When the magnetic field was applied perpendicular to plane, however the loop was almost reversible. As a result, both S and H_c are close to zero. Therefore, it is obvious that the easy magnetization axis of Co film lays in-plane while hard axis is perpendicular to plane.

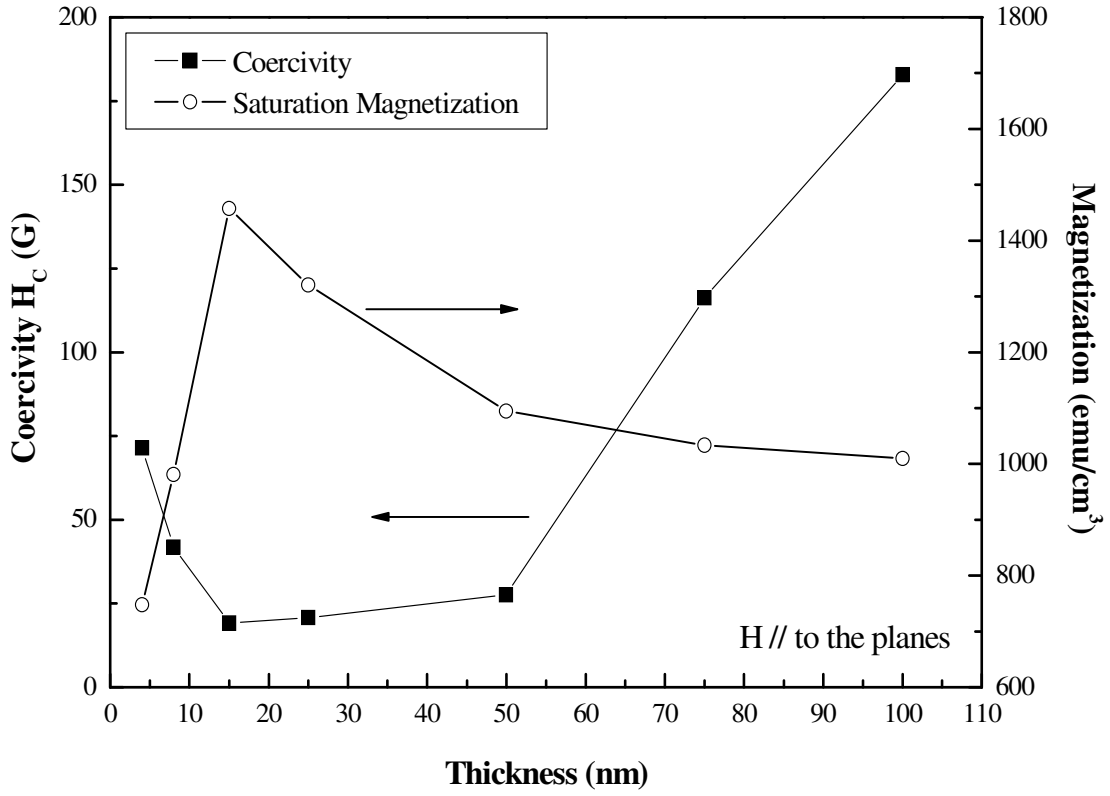

Figure 4.23. The thickness dependence of coercivity and saturation magnetization of Co films on Si(100) substrate. Applied field *H* is parallel to the film plane.

In order to study the magnetic properties further, we prepared series of thinner films which have 4, 8, 15, 25, 50, 75 and 100 nm thicknesses. For each sample the hysteresis loop was recorded as of magnetic field in the plane of the film. The thickness dependence of H_c and M_s of the films are shown in Fig. 4.23. By comparing the results, it is clear that the H_c and M_s depend strongly on the film thickness (Munford 2001, Li 2000). According to the measurements, the H_c of the Co films is decreasing with increasing film thickness up to a threshold value which is between 15 and 25 nm. This low observed H_c value indicates the soft magnetic nature of thin Co film. It is known that the thin film structures contain various point defects and stresses, which are released as the thickness of the film is increased. With further increase of the thickness up to 100 nm, H_c increased almost linearly as reported in 2007 (Islam et al. 2007). The H_c reached the value of 180 G, which was about 9 times larger than its minimum value (~19 G). The observed increase in H_c at higher thicknesses of Co thin film is mainly due to the increase in grain size. It is well known that when the crystal grains are large,

crystalline magnetic anisotropy is large and magnetization in each crystal grain orient in different direction, because easy axis are not parallel to each other. In this case magnetization cannot rotate at the same time and the hysteresis in the *M-H* character become large and soft magnetic properties become poor (Sharma 2007).

The saturation magnetization (M_s) for different thicknesses of layers (4, 8, 15, 25, 50, 75 and 100 nm) are 748, 981, 1458, 1321, 1095, 1034, and 1010 emu/cm^3, respectively, which are dependent on thickness and grain size. Calculation of high magnetization values can be because of the sensitivity of thickness measurement. Existence of point defects in thinner films might be the reason of low magnetization values. The magnetization of 15 nm Co film reaches its maximum value which is close to magnetization of bulk Co (1422 emu/cm^3). In small grains, magnetization can be rotated easily by applying low magnetic fields (Deo et al. 2005). After this critical thickness (15 nm), grain size and crystallinity of Co films increase. However, it will be more difficult to rotate the magnetization totally in each large grain causing low magnetization values.

After determining the critical thickness, we deposited Si/Co(4nm) films with different growth pressures (0.5, 1.3, 3.0, and 5.0 mTorr) in order to have the highest H_c for thin Co layer. The hysteresis loops of the samples are shown in Fig. 4.24. As the growth pressure increases, the H_c increases whereas the magnetization of the samples decreases. At low pressures, H_c is low due to the high energetic sputtered atoms which cause large grains and smooth films. Therefore, it is easy to rotate the magnetization with low magnetic fields for these films and they have high magnetization values. Here, the Co film with 3.0 mTorr pressure has the highest H_c, so it might be convenient to use it for pinned ferromagnetic electrode in MTJ stack.

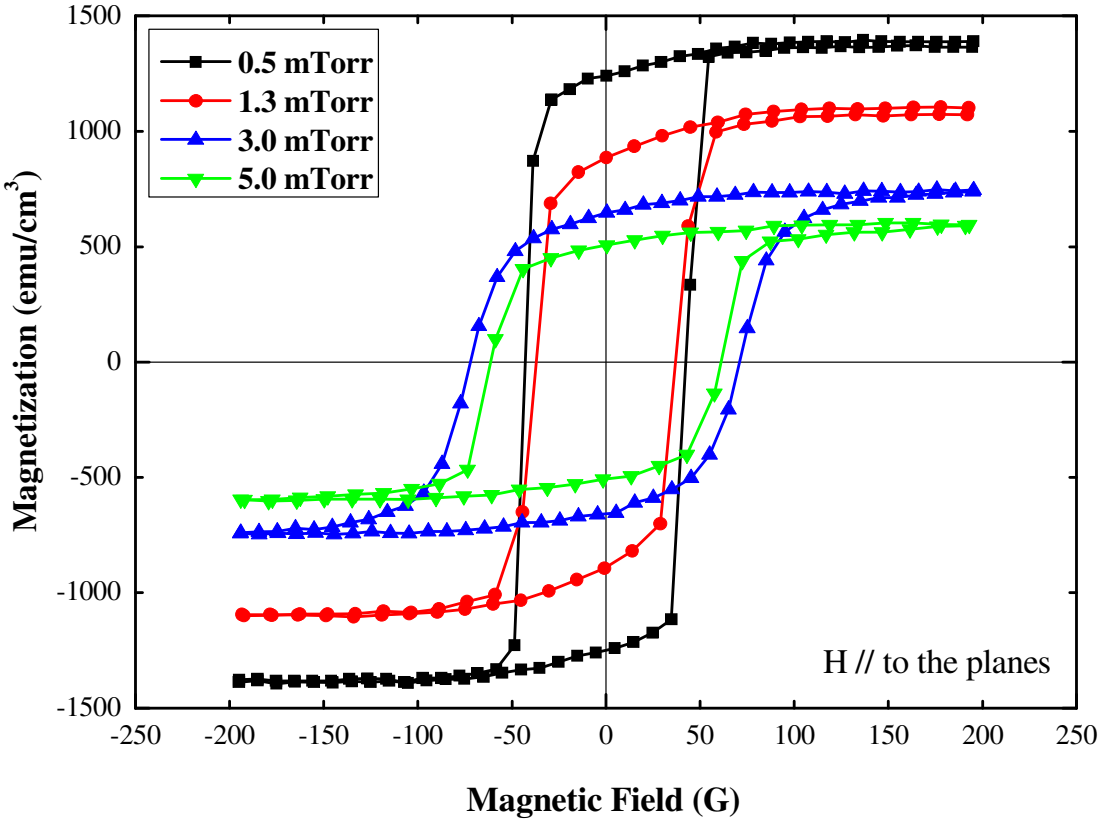

Figure 4.24. Hysteresis loops of Si/Co(4nm) samples with different deposition pressures.

Tantalum buffer layer is used for contact layer in order to carry out magnetoresistance (MR) measurements in MTJ structures for spintronics applications. Therefore, we deposited Si/Ta(7nm)/Co(4nm) thin bilayers with changing the deposition pressure of Co layers in order to investigate how the magnetic properties of Co change when it is grown on Ta layer. We did not use 100 nm film for Co which have very high H_c because we need very thin films for MTJ structures. The hysteresis loops for the samples are shown in Fig. 4.25. It is obvious that with increasing Co pressure, the coercivity of the samples increases. The effects of pressure have been described in section 2.1. Having low Ar pressure causes denser and smoother films because of the more energetic sputtered atoms. Therefore, the samples with low pressures have larger grain size than the samples which were deposited at higher pressures. These larger grains are the reason for low H_c. The deposition pressures of Cobalt were 0.5 mTorr, 1.3 mTorr, 3.0 mTorr and 5.0 mTorr and the H_c values are 23 G, 34 G, 42 G and 69 G, respectively.

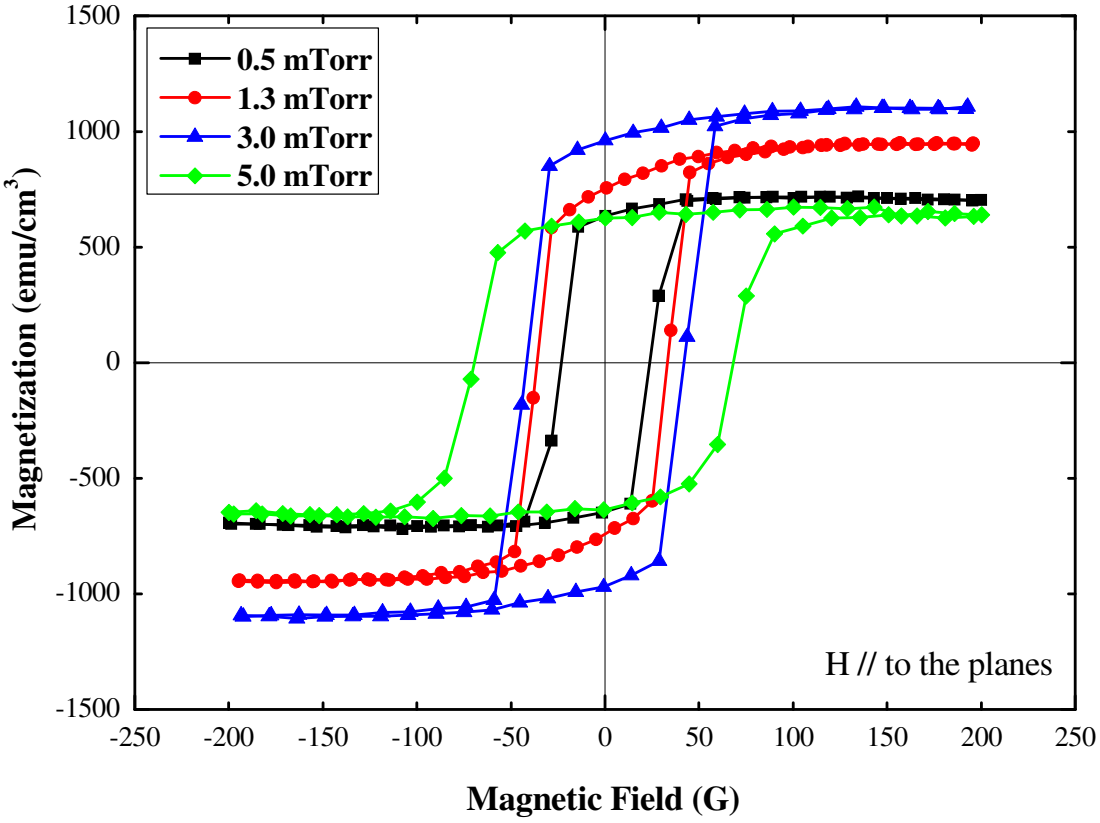

Figure 4.25. Hysteresis loops of Si/Ta(7nm)/Co(4nm) samples with deposited Co at different pressures.

In addition, the magnetization also increases with deposition pressure. However, the sample with 5 mTorr pressure has the lowest magnetization value. This might be the result of having rougher surface which can cause demagnetizing fields.

After studying thin Co layer at different pressures, we also investigated Ta/Co bilayers with changing thicknesses of both Co and Ta layers. The hysteresis curves of Si/Ta(7nm)/Co(4nm), Si/Ta(7nm)/Co(25nm), Si/Ta(40nm)/Co(4nm) and Si/Ta(40nm)/ Co(25nm) are shown in Fig. 4.26 with H_c values. We noticed from these hysteresis loops that the sample which includes thick Ta and Co gave us very low H_c (18 G). Therefore, it is more convenient to use thick Ta and Co films for free layer of MTJ stack.

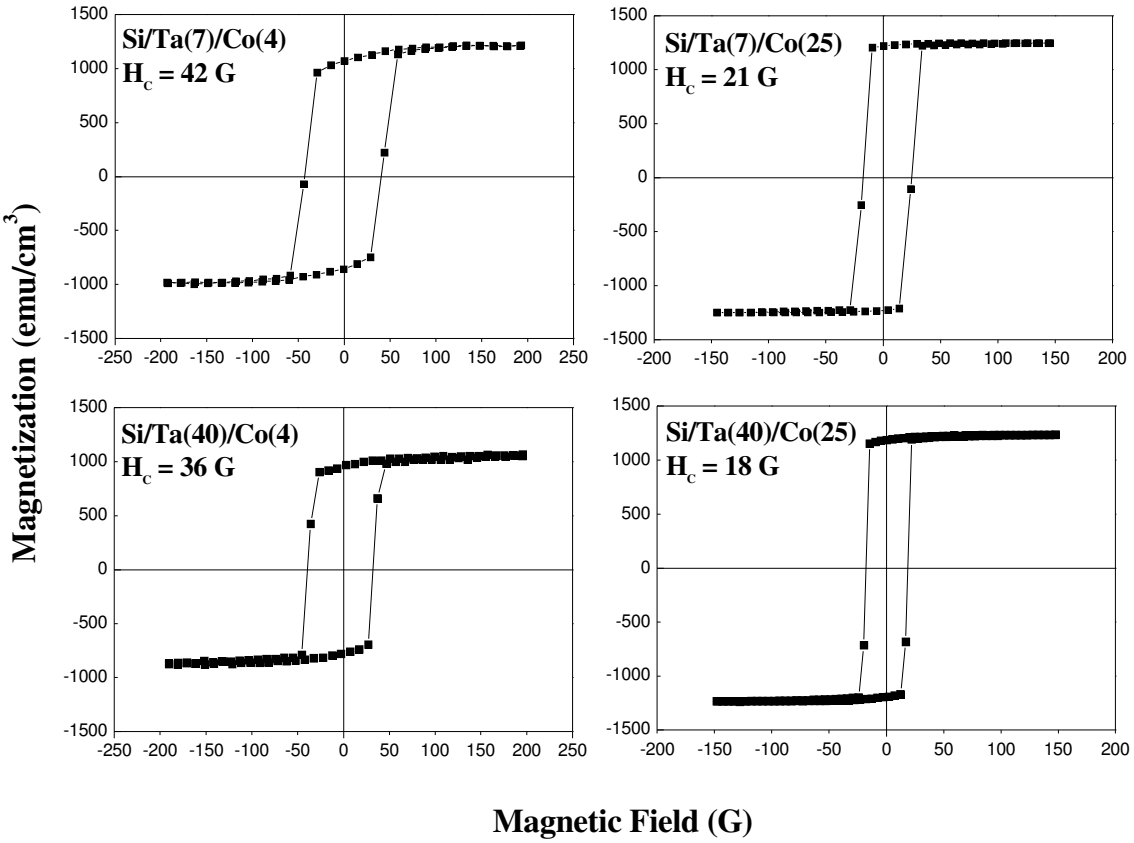

Figure 4.26. Hysteresis curves for Si/Ta/Co bilayers with different layer thicknesses.

Another interesting point is that when we changed the Ta thickness without changing Co thickness, the H_c value did not change much. Thick Ta just makes the crystallinity of Co better and it is good to have thick bottom contact layer. If we increase Co thickness while the Ta thickness is fixed, the H_c decreases and high squareness is obtained as expected. It can be inferred from the quality of squareness that for applied magnetic field in the direction of easy axis of magnetization, hysteresis curve is a perfect square suggesting that the magnetization takes place purely through domain wall motion (Kumar and Gupta 2007).

In order to study multilayers for MTJ purposes, we first grew the following GMR stack: Si/Ta(40nm)/Co(25nm)/Ta(7nm)/Co(4nm)/Ta(7nm) where the Ta layer between two magnetic electrodes is used for the barrier. The last thin Ta layer is a contact and a capping layer for keeping top Co layer from oxidation. Using VSM, the hysteresis loop which is shown in Fig. 4.27 was obtained. In MTJs, free and pinned magnetic layers should change their magnetization alignments independently due to the magnetic field. Therefore, two different coercivity steps have to be seen in the hystresis

curve. However, because of the coupling between the ferromagnetic layers we do not have any steps for this structure. Coupling prevents the magnetic layers from rotating their magnetizations without affecting each other. Since Ta is a metal, the coupling occurs due to the itinerant (conduction) electrons. This effect is called Ruderman-Kittel-Kasuya-Yosida (RKKY) interaction (Ruderman 1954, Kasuya 1956, Yosida 1957).

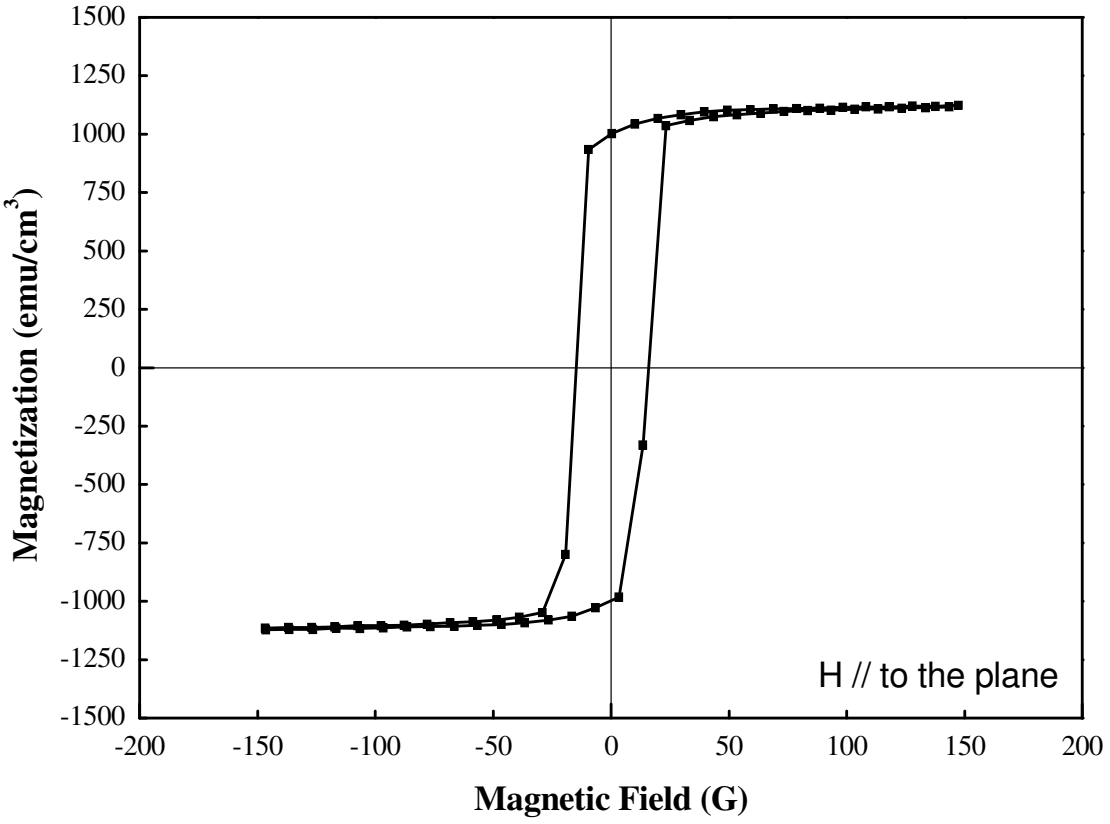

Figure 4.27. Magnetic hysteresis curve for Si/Ta(40nm)/Co(25nm)/Ta(7nm)/Co(4nm)/ Ta(7nm).

After this sample, 7 nm Ta_2O_5 insulator layer was replaced with the conductor layer in order to have MTJ structure. The hysteresis graph of this structure is shown in Fig. 4.28. The shape of the curve obviously indicates that there are two magnetic phases with different H_c in multilayer. When the magnetic field H is in the range of 70-100 G, one Co layer keeps the original orientation and the other turns to opposite orientation. The adjacent magnetic layers are in anti-parallel alignment. This forms a hard-soft system (Ma and Wong 2002).

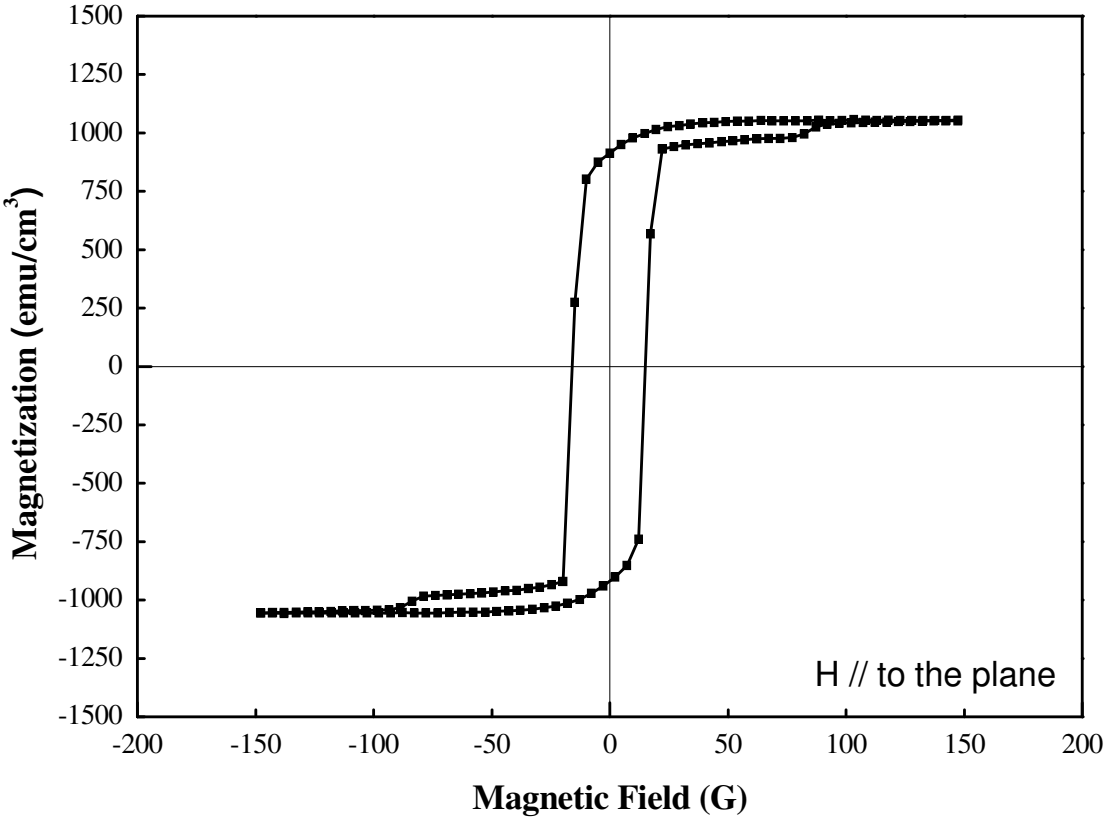

Figure 4.28. Magnetic hysteresis curve for Si/Ta(40nm)/Co(25nm)/Ta_2O_5(7nm)/Co (4nm)/Ta(7nm).

For further work, the thicknesses of Ta_2O_5 and Co layers will be changed to achieve clear magnetic phases. After having the successful MTJ structure, the magnetoresistance measurements will be carried out for spintronics device applications.

CHAPTER 5

CONCLUSION

Si(100)/Ta/Co magnetic multilayer structures were grown by UHV Magnetron Sputtering System. XRD analysis showed that single Co layer grows amorphous on silicon substrate up to 50 nm and then starts crystallizing with (100), (002), and (101) orientations at $2\theta = 41.68^0$, 44.53^0, and 47.41^0, respectively. The grain size increases as the thickness of film increases. After annealing 25 nm amorphous Co film at 450^0C at high vacuum, a peak was observed at $2\theta = 44.75^0$ which shows a transformation from amorphous to single crystalline hexagonal (002) phase with 27 nm grain size. Single Ta layer with thickness of 40 nm has a good quality single crystalline structure of tetragonal tantalum (β-Ta) phase with (002) plane at $2\theta = 33.98^0$. The XRD spectrum of Ta/Co bilayers and MTJ stacks also gave us good crystallinity for Co and Ta layers without annealing.

AFM surface roughness measurements of the samples were performed and it is revealed that with increasing Co film thickness on silicon substrate, the rms roughness value first increases up to 5.6 Å for 15 nm film, and then decreases with increasing thickness. This is because of the crystallization of Co after 25 nm and increasing grain sizes with thickness. The rms roughness values for 40 and 80 nm Ta single layers were found to be increasing with thickness to 0.9 Å and 2.2 Å, respectively. These low values might be the result of low lattice mismatch (6.13%) between tantalum and silicon substrate. In Ta/Co bilayers, when Co layer thickness is increased, surface rms roughness value decreases. According to XRD results, cobalt grows good quality single crystal on tantalum, so the surface is uniform and homogeneous. SEM cross-section images also showed that we have uniform and continuous film growth on silicon substrate for both single and bilayers. However, because of the resolution of our SEM, we could not investigate the very thin films.

The hysteresis loops of all samples were determined by using VSM. From the azimuthal angle measurements, Co films showed in-plane easy axis magnetization. The thickness dependence of coercivity (H_c) and saturation magnetization (M_s) was investigated. When the thickness of Co film on silicon substrate was increased from 4 nm to 15 nm, the H_c value decreased from 72 G to 20 G. Thin films might have point

defects and stresses which are released as the thickness of the film is increased. After 25 nm, the H_c increases almost linearly up to 180 G for 100 nm Co film. This increase in H_c and decrease in M_s are due to the formation of large grains and crystallinity of cobalt. 15 nm Co sample has the highest magnetization value which is close to bulk Co magnetization (1422 emu/cm^3). After having high H_c value for thin Co layer, we deposited Co films on silicon for different deposition pressures. It is found that with increasing pressure, the H_c values also increased. This might be the reason of the low deposition pressure which causes denser and smoother films because of more energetic sputtered atoms. Thus, the films with low pressures have larger grain size than the samples which were deposited at higher pressures. We have also changed the deposition pressure of Co layer deposited on Ta layer. The H_c increased again with the increasing Co deposition pressure. In order to understand thickness dependency better, we grew Ta/Co bilayers which have different Co and Ta thicknesses. When only the Co thickness increased, the H_c of the sample decreased as expected. However, the interesting point is that only changing Ta layer thickness does not make any difference in H_c of the sample. The lowest H_c value (18 G) was found for Si/Ta(40nm)/Co(25nm) bilayer. Then, we constructed Si/Ta/Co/Ta/Co/Ta multilayer where Ta metal is used as a barrier layer between the ferromagnetic electrodes. For this GMR structure, there was no coercivity steps observed in the hysteresis because coupling which is due to RKKY interaction prevents the magnetizations of the magnetic layers from rotation independently. Finally, we produced Si/Ta/Co/Ta_2O_5/Co/Ta multilayer for MTJ purposes. The hysteresis curve of this sandwich gave us two magnetic phases with different H_c in multilayer which forms a hard-soft system.

For future work, the thicknesses of Co and Ta_2O_5 layers will be changed in order to achieve clear coercivity steps. Moreover, the samples will be patterned to carry out magnetoresistance measurements for investigation of spintronics applications.

REFERENCES

Ali, M., 1999. "Growth and Study of Magnetostrictive FeSiBC Thin Films for Device Applications", Ph.D.'s Thesis, The University of Sheffield.

Andersson, C., 2006. "Exploring the Magnetism of Ultra Thin 3d Transition Metal Films", Ph.D.'s Thesis, Uppsala University.

Baibich, M.N., Broto, J.M., Fert, A., Nyugen Van Dau, F., Petroff, F., Eitenne, P. Creuzet, G., Friederich, A., and Chazelas, J. 1988. "Giant Magnetoresistance of (001)Fe/(001)Cr Magnetic Superlattices", *Physical Review Letters*. Vol. 61, No. 21, p. 2472.

Barthélémy, A., Fert, A., Contour, J-P., Bowen, M., Cros, V., De Teresa, J.M., Hamzic, A., Faini, J.C., George, J.M., Grollier, J., Montaigne, F., Pailloux, F., Petroff, F. and Vouille, C. 2002. "Magnetoresistance and Spin Electronics", *Journal of Magnetism and Magnetic Materials*. Vol. 242-245, p. 68.

Bensmina, B., Humbert, P., Dinia, A., Muller, D., Speriosu, V.S., Gurney, B.A. 1999. "Annealing Effect on the Magnetic Properties of Ta 50 Å/Cu 50 Å/Co 75 Å/Cu 50 Å/ Ta 50 Å Sandwiches", *Journal of Magnetism and Magnetic Materials*. Vol. 198-199, pp. 338-340.

Binasch, G., Grünberg, P., Saurenbach, F., Zinn, W. 1989. "Enhanced Magnetoresistance in Layered Magnetic Structures with Antiferromagnetic Interlayer Exchange", *Physical Review B*. Vol. 39, No. 7, pp. 4828-4830.

Cheng, H.-E., Mao, C.-T. 2003. "The Effect of Substrate Temperature on the Physical Properties of Tantalum Oxide Thin Films Grown by Reactive Radio-Frequency Sputtering" *Materials Research Bulletin*. Vol. 38, pp. 1841-1849.

Cullity, B.D. and Stock, S.R., 2001. *Elements of X-Ray Diffraction*, (Prentice Hall, New Jersey), pp. 103-184.

Demiryont, H., Sites. J.R. and Geib, K. 1985. "Effects of Oxygen Content on the Optical Properties of Tantalum Oxide Films Deposited by Ion-Beam Sputtering", *Applied Optics*. Vol. 24, No. 4, p. 490.

Deo, N., Bain, M.F., Montgomery, J.H., Gamble, H.S. 2005. "Study of Magnetic Properties of Thin Cobalt Films Deposited by Chemical Vapour Deposition", *Journal of Material Science*: *Materials in Electronics*. Vol. 16, pp. 387-392.

Entani, S., Kiguchi, M., Ikeda, S., Saiki, K. 2005. "Magnetic Properties of Ultrathin Cobalt Films on SiO_2 Substrates", *Thin Solid Films*. Vol. 493, pp. 221-225.

Hoogeveen, R., Moske, M., Geisler, H., Samwer, K. 1996. "Texture and Phase Transformation of Sputter-deposited Metastable Ta Films and Ta/Cu Multilayers", *Thin Solid Films*. Vol. 275, pp. 203-206.

Islam, J., Yamamoto, Y. Hori, H. 2007. "Thickness-dependent Coercivity and Magnetization Process of Co/GaAs (100)", *Journal of Magnetism and Magnetic Materials*. Vol. 310, pp. 2234-2236.

Jiang, A., Yohannan, A., Nnolim, N.O., Tyson, T.A., Axe, L., Lee, S.L., Cote, P. 2003. "Investigation of the Structure of β-Tantalum", *Thin Solid Films*. Vol. 437, pp. 116-122.

Julliere, M. 1975. "Tunneling Between Ferromagnetic Films", *Physics Letters*. Vol. 54A, No. 3, p. 225-226.

Kasuya, T. 1956. "A Theory of Metallic Ferro- and Antiferromagnetism on Zener's Model", *Progress of Theoretical Physics*. Vol. 16, pp. 45-57.

Kharmouche, A., Chérif, S.-M., Bourzami, A., Layadi, A., Schmerber, G. 2004. "Structural and Magnetic Properties of Evaporated Co/Si(100) and Co/Glass Thin Films", *Journal of Physics D: Applied Physics*. Vol. 37, pp. 2583-2587.

Knechten, C.A.M., 2004. "Plasma Oxidation for Magnetic Tunnel Junctions", Ph.D.'s Thesis, Eindhoven University of Technology.

Kohli, S., McCurdy, P.R., Rithner, C.D., Dorhout, P.K., Dummer, A.M., Brizuela, F., Menoni, C.S. 2004. "X-Ray Characterization of Oriented β-Tantalum Films", *Thin Solid Films*. Vol. 469-470, pp. 404-409.

Kumar, D., Gupta, A. 2007. "Evolution of Structural and Magnetic Properties of Sputtered Nanocrystalline Co Thin Films with Thermal Annealing", *Journal of Magnetism and Magnetic Materials*. Vol. 308, pp. 318-324.

Kumar, G., 2005. "Structural and Magnetic Characterization of Nd-based Nd-Fe and Nd-Fe-Co-Al Metastable Alloys", Ph.D.'s Thesis, Technical University Dresden.

Lee, S.L., Doxbeck, M., Mueller, J., Cipollo, M., Cote, P. 2004. "Texture, Structure and Phase Transformation in Sputter Beta Tantalum Coating", *Surface and Coatings Technology*. Vol. 177-178, pp. 44-51.

Lee, Y.-M., Hayakawa, J., Ikeda, S., Matsukura, F., Ohno, H. 2007. "Effect of Electrode Composition on the Tunnel Magnetoresistance of Pseudo-spin-valve Magnetic Tunnel Junction with a MgO Tunnel Barrier", *Applied Physics Letters*. Vol. 90, No. 212507, pp. 1-3.

Li, M., Wang, G.-C. 2000. "In Situ Measurement of Thickness Dependence of Magnetoresistance and Magnetic Hysteresis Loops of Ultrathin Co Films on a SiO_2/Si(111) Substrate", *Journal of Magnetism and Magnetic Materials*. Vol. 217, pp. 199-206.

Liu, L., Gong, H., Wang, Y., Wang, Y., Wee, A.T.S., Liu, R. 2001. "Annealing Effects of Tantalum Thin Films Sputtered on [001] Silicon Substrate", *Materials Science and Engineering C*. Vol. 16, pp. 85-89.

Ma, B., Wong, C.Y., 2002. "Giant Magneto-resistance of Co/Cu/Co Sandwich with Buffer Layers and CPP Transport Multilayer", 8th International Conference on Electronic Materials (IUMRS-ICEM 2002, Xi'an, China, 10-14 June 2002).

Maeng, S., Axe, L., Tyson, T.A., Cote, P. 2006. "Corrosion Behaviour of Electrodeposited and Sputtered Cr Coatings and Sputtered Ta Coatings with α and β Phases", *Surface & Coatings Technology*. Vol. 200, pp. 5767-5777.

Materne, A., Moriceau, H., Blanchard, B., Florestan, J. 1988. "Changes in Stress and Coercivity After Annealing of Amorphous Co(Zr, Nb) Thin Films Deposited by RF Sputtering", *IEEE Transactions on Magnetics*. Vol. 24, pp. 1752-1754.

Mitsuzuka, T., Matsuda, K., Kamijo, A., and Tsuge, H. 1999. "Interface Structures and Magnetoresistance in Magnetic Tunnel Junctions", *Journal of Applied Physics*. Vol. 85, No. 8, p. 5807.

Mohite, V., 2004. "Self Controlled Magnetic Hyperthermia", M.Sc.'s Thesis, The Florida State University.

Moodera, J.S., Kinder, L.R., Wong, T.M. and Meservey, R. 1995. "Large Magnetoresistance at Room Temperature in Ferromagnetic Thin Film Tunnel Junctions", *Physical Review Letters*. Vol. 74, No. 16, p. 3273.

Munford, M.L., Seligman, L., Sartorelli, M.L., Voltolini, E., Martins, L.F.O., Schwarzacher, W., Pasa, A.A. 2001. "Electrodeposition of Magnetic Thin Films of Cobalt on Silicon", *Journal of Magnetism and Magnetic Materials*. Vol. 226-230, pp. 1613-1615.

Ng, V., Hu, J.F., Adeyeye, A.O., Wang, J.P., Chong, T.C. 2002. "Radio Frequency Substrate Bias Effect on Properties of Co Thin Film and Multilayer Structures", *Journal of Magnetism and Magnetic Materials*. Vol. 247, pp. 339-344.

Prinz, G.A. 1998. "Magnetoelectronics", *Science's Compass Review*. Vol. 282, pp. 1660-1663.

Ranganathan, R.P., 2004. "Effects of Deposition Temperature and Post Deposition Annealing on the Electrical Properties of Barium Strontium Titanate Thin Film for Embedded Capacitor Applications", M.Sc.'s Thesis, University of Central Florida Orlando.

Rao, N.R., Chandramani, R., Rao, G.M. 1999. "Tantalum Oxide Films Prepared by Unbalanced Reactive Magnetron Sputtering", *Journal of Materials Science Letters*. Vol. 18, pp. 1949-1951.

Read, M.H., Altman, C. 1965. "A New Structure in Tantalum Thin Films", *Applied Physics Letters*. Vol. 7, pp 51-52.

Rijks, T.G.S.M., Coehoorn, R., de Jong, M.J.M., de Jonge, W.J.M. 1995. "Semiclassical Calculations of the Anisotropic Magnetoresistance of NiFe-based Thin Films, Wires, and Multilayers", *Physical Review B*. Vol. 51, No. 1, pp. 283-291.

Roy, R.A., Catania, P., Saenger, K.L., Cuomo, J.J., Lossy, R.L. 1993. "Role of Energetic Atoms and Ions in Ta Films Grown by Different Physical Vapor Deposition Methods", *Journal of Vacuum Science and Technology B*. Vol. 11, pp. 1921-1927.

Ruderman, M.A., Kittel, C. 1954. "Indirect Exchange Coupling of Nuclear Magnetic Moments by Conduction Electrons", *Physical Review*. Vol. 96, pp. 99-102.

Sharma, A., Brajpuriya, R., Tripathi, S., and Chaudhari, S. M. 2006. "Study of Annealed Co Thin Films Deposited by Ion Beam Sputtering", *Journal of Vacuum Science and Technology A*. Vol. 24. pp. 74.

Sharma, A., Tripathi, S., Brajpuriya, R., Shripathi, T., and Chaudhari, S. M. 2007. "Thickness Dependent Structural, Magnetic and Transport Properties of Nanostructured Cobalt Thin Films", *Journal of Nanoscience and Nanotechnology*. Vol. 7. pp. 2041-2045.

Silva, L.M.A., 2006. "Study of Structural, Electrical, Optical and Magnetic Properties of ZnO Based Films Produced by Magnetron Sputtering", M.Sc.'s Thesis, University of Puerto Rico.

Smits, A.A., 2001. "Tunnel Junctions: Noise and Barrier Characterization", Ph.D.'s Thesis, Eindhoven University of Technology.

Somekh, R.E. 1984. "The Thermalization of Energetic Atoms During the Sputtering Process", *Journal of Vacuum Science and Technology A*. Vol. 2, pp. 1285-1291.

Tay, M., Li, K., Wu, Y. 2005. "Electrical Transport Properties of Ultrathin Metallic Films", *Journal of Vacuum Science and Technology B*. Vol. 23, pp. 1412-1416.

Thomson, W. 1856. "On the Electro-dynamic Qualities of Metals: Effects of Magnetization on the Electric Conductivity of Nickel and of Iron", *The Royal Society of London*. Vol. 8, pp. 546-550.

Tiusan, C., Hehn, M., Ounadjela, K. 2002. "Magnetic-roughness-induced Magnetostatic Interactions in Magnetic Tunnel Junctions", *The European Physical Journal B*. Vol. 26, pp. 431-434.

Turner, T.L., 2001. "Investigation of the Properties of Magnetic Films Deposited on Carbon Nitride", B.S.'s Thesis, College of William and Mary in Virginia.

Wang, D., Nordman, C., Daughton, J.M., Qian, Z., Fink, J. 2004. "70% TMR at Room Temperature for SDT Sandwich Junctions with CoFeB as Free and Reference Layers", *IEEE Transactions on Magnetics*. Vol. 40, No. 4, pp. 2269-2271.

Wang, Y.C., Ding, J., Yi, J.B., Liu, B.H., Yu, T., Shen, Z.X. 2004. "High coercivity Co-ferrite Thin Films on SiO_2 (100) Substrate", *Journal of Magnetism and Magnetic Materials*. Vol. 282, pp. 211-215.

Warot-Fonrose, B., Traverse, A., Calmels, L., Serin, V., Snoeck, E. 2006. "Structural and magnetic studies of Co thin films", *Micron*. Vol. 37. pp. 478-485.

Wasa, K., Kitabatake, M., Adachi, H., 2004. *Thin Film Materials Technology.* (William Andrew, Inc., New York)

WEB_1, 2007. X-Ray Diffraction, Department of Earth & Planetary Sciences, 26/04/2007. http://epswww.unm.edu/xrd/

WEB_2, 2007. Patent Storm, 30/07/2007. http://www.patentstorm.us/patents/6133086-description.html

Wieldraaijer, H., 2006. "Ultrathin Co Films for Magnetoresistive Devices: An NMR Study", Ph.D.'s Thesis, Eindhoven University of Technology.

Wu, Y. 2003. "Nano Spintronics for Data Storage", *Encyclopedia of Nanoscience and Nanotechnology*. Vol. X, pp. 1-50.

Wu, Y.-E., Tsay, J.-S., Chen, S.-C., Fu, T.-Y., Shern, C.-S. 2001. "Magnetic Properties of Co/Si(100) Thin Films Studied Using Magnetooptic Kerr Effect Technique", *Japanese Journal of Applied Physics*. Vol. 40, pp. 6825-6828.

Yosida, K. 1957. "Magnetic Properties of Cu-Mn Alloys", *Physical Review*. Vol. 106, pp. 893-898.